

Fermi National Accelerator Laboratory

FERMILAB-TM-2046

**Performance of the KTeV High-Energy Neutral Kaon Beam at
Fermilab**

V. Bocean et al.

*Fermi National Accelerator Laboratory
P.O. Box 500, Batavia, Illinois 60510*

June 1998

Performance of the KTeV High-Energy Neutral Kaon Beam at Fermilab

V. Bocean, S. Childress, R. Coleman, R. Ford,
G. Gutierrez, D. Jensen, T. Kobilarcik, R. Tokarek

March 20, 1998

The performance of the primary and secondary beams for the KTeV experiments E832 and E799-II is reviewed. The beam was commissioned in the summer of 1996 and initially operated for approximately one year. The report includes results on the primary beam, target station including primary beam dump and muon sweeping system, neutral beam collimation system, and alignment.

1. Introduction

KTeV is an experimental program currently consisting of two experiments: E832 and E799-II. E832 is an experiment to perform a high accuracy measurement of CP violation ($\epsilon'/\epsilon \sim 10^{-4}$). The secondary beams are two neutral horizontally-separated square beams. In E832 a regenerator alternates between the beams every spill. The regenerator beam is used to re-create K_S^0 from an almost pure K_L^0 beam. E799-II is an experiment to perform a search and/or study of neutral kaon and hyperon rare decays occurring in either beam in the 60 meter vacuum decay region. The "KTeV Design Report" gives a complete description¹ of KTeV. Figures 1 and 2 give a plan and 3D view of the detector.

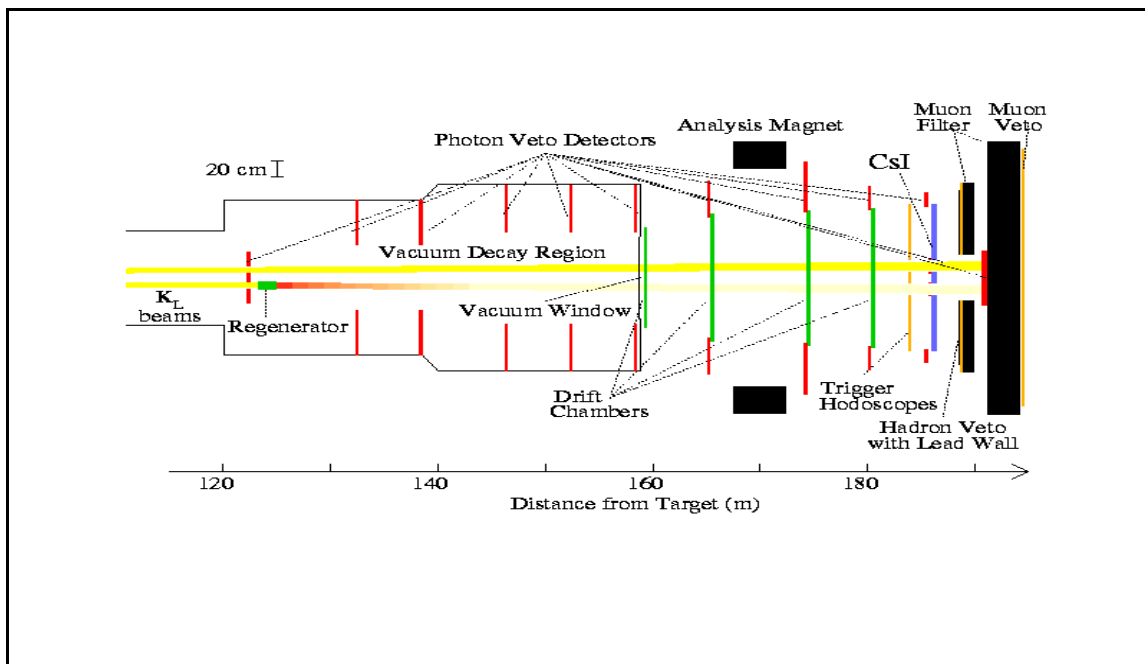


Fig. 1. Plan view of KTeV E832 detector configuration

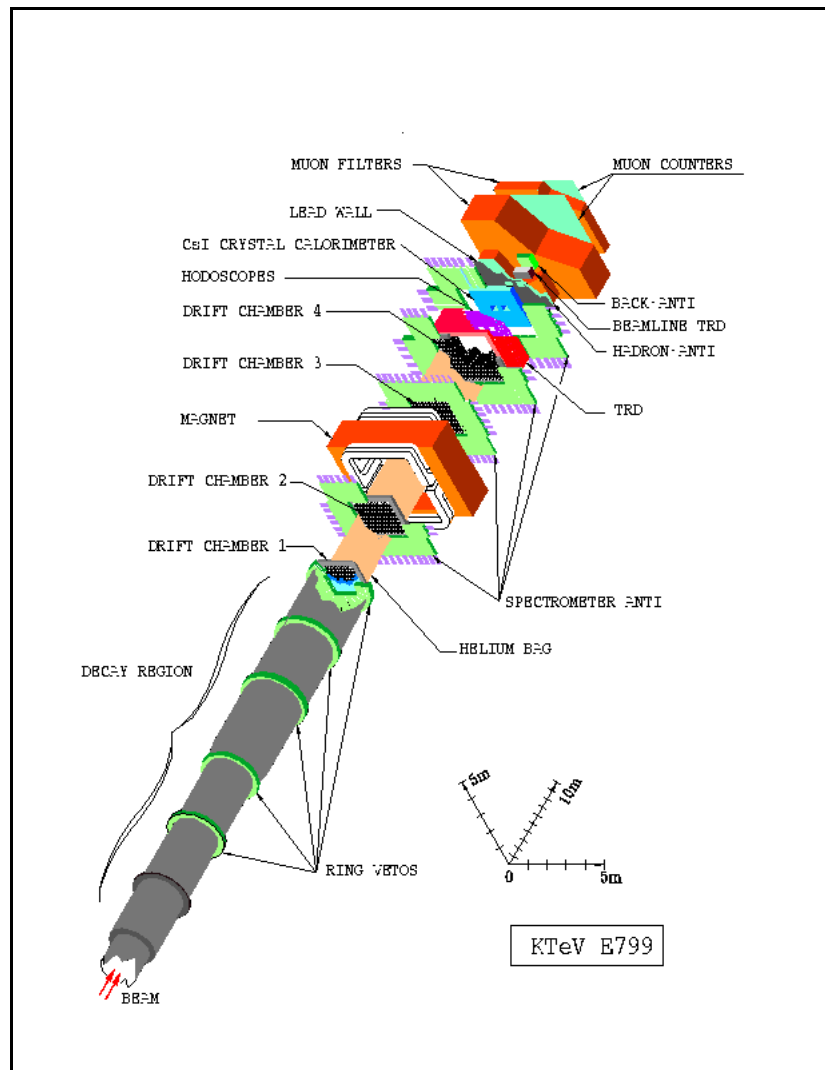


Fig. 2. 3-D view of KTeV E799-II detector configuration

Much of the direction for building the new KTeV beamline came from our experience in the Meson Center neutral kaon program in which data was collected from 1987-1991². The new KTeV beamline required several major improvements over the Meson Center beam. The areas of concern in the Meson Center beam which affected the data taking and physics analysis are listed below:

- **Primary beam stability**

The position of the primary beam varied in the vertical plane depending on the intensity (~600 microns). This effect added

smearing effects on the neutral beam profiles at the detector³. Also the tuning of the primary beam was manually controlled.

- **Muon rates from the target/dump**

The muon rates in the detector operating with $\sim 1 \times 10^{12}$ incident protons per spill were ~ 1 -2 MHz/m² adding extra tracks to the physics events. The muon rates in the counting house area limited the amount of protons on target to about 2×10^{12} per Tevatron cycle.

- **Neutral beam halo**

In these Meson Center experiments, the two neutral beams passed through beam holes in the lead-glass calorimeter. Neutral halo caused large radiation damage in the crystals near the beam (~ 100 to 600 rads/week). A large software effort in the physics analysis was required to track the calibration and systematics introduced by this radiation damage. One cause of this neutral halo was a target-collimation system in which some components in the heavily shielded target station were not adjustable. Shifts in the floor elevation of 1.25 cm compromised the collimation system. In addition the combination of poorly machined collimators and component misalignments allowed multiple scattering in the necessary absorber to create neutral halo. Finally, the lack of beam holes in a trigger hodoscope just upstream of the calorimeter created interactions with the neutral beam which added an amount of radiation damage comparable to the neutral halo.

The specification and design of the new beamline is documented in Ref. 4. The goal was to reduce the problems discussed above to a level below which they would compromise the physics, particularly the high precision CP violation experiment E832. In addition higher intensity beams were required. The resulting requirements on the primary beam are listed in the table below:

Table 1. Primary Beam Specification

Proton beam energy	800 GeV
Proton intensity	5×10^{12} protons per 20 sec spill
Length of run	1 year
Targeting angle	-4.8 mrad (vertical); < 0.02 mrad (horizontal)
Targeting angle variability	-4.0 to -5.6 mrad (vertical)
Beam size at the target (σ)	$\leq 250 \mu\text{m}$ (horizontal and vertical)
Beam spot stability	$\leq \pm 50 \mu\text{m}$ (horizontal and vertical)
Beam position stability	$\leq \pm 100 \mu\text{m}$ (horizontal and vertical)
Beam angle stability	$\leq \pm 25 \mu\text{rad}$ (horizontal and vertical)

The goal for muon rates in the spectrometer from the primary and beam dump sources was less than 100 kHz for 5×10^{12} incident protons per spill. This is less than the projected inherent muon rate from kaon decays. The radiation level at the experimental counting room should also be well within specified personnel safety levels, as should outdoor area muon rates.

The requirements on the symmetry and alignment of the two neutral beams were quite challenging. Not only did the collimators which formed the secondary beam have to be both machined and aligned precisely, their positions also had to be stable in time.

Table 2. Secondary Neutral Beam Specification

Separation of beams	± 15 cm at CsI (186m from target) horiz. center-to-center
X,Y angular divergence	± 0.250 mrad
Solid Angle	0.250 microsteradians
Size at CsI	9.30 cm x 9.30 cm
Tolerance on Size and Position at CsI	<0.5 mm
Areas of two beams	equal within 1%
Alignment of target-collimation components	± 200 microns

The experiment and associated beamlines are underground in two essentially isolated enclosures, as shown in fig. 3. The primary beam, the target, and part of the secondary (neutral) beam are contained in one enclosure (NM2). Subsequent components of the neutral beam and the experiment are contained in a pair of contiguous newly built enclosures (NM3/4). Beam transport between enclosures NM2 and NM3 is made possible through a buried 30 cm diameter beam pipe. Additionally, a 30 cm diameter horizontal sight pipe has been installed to provide direct visibility between enclosures for alignment purposes. These pipes are surrounded by a 2.4 m x 2.4 m steel muon shield of 10 m in length.

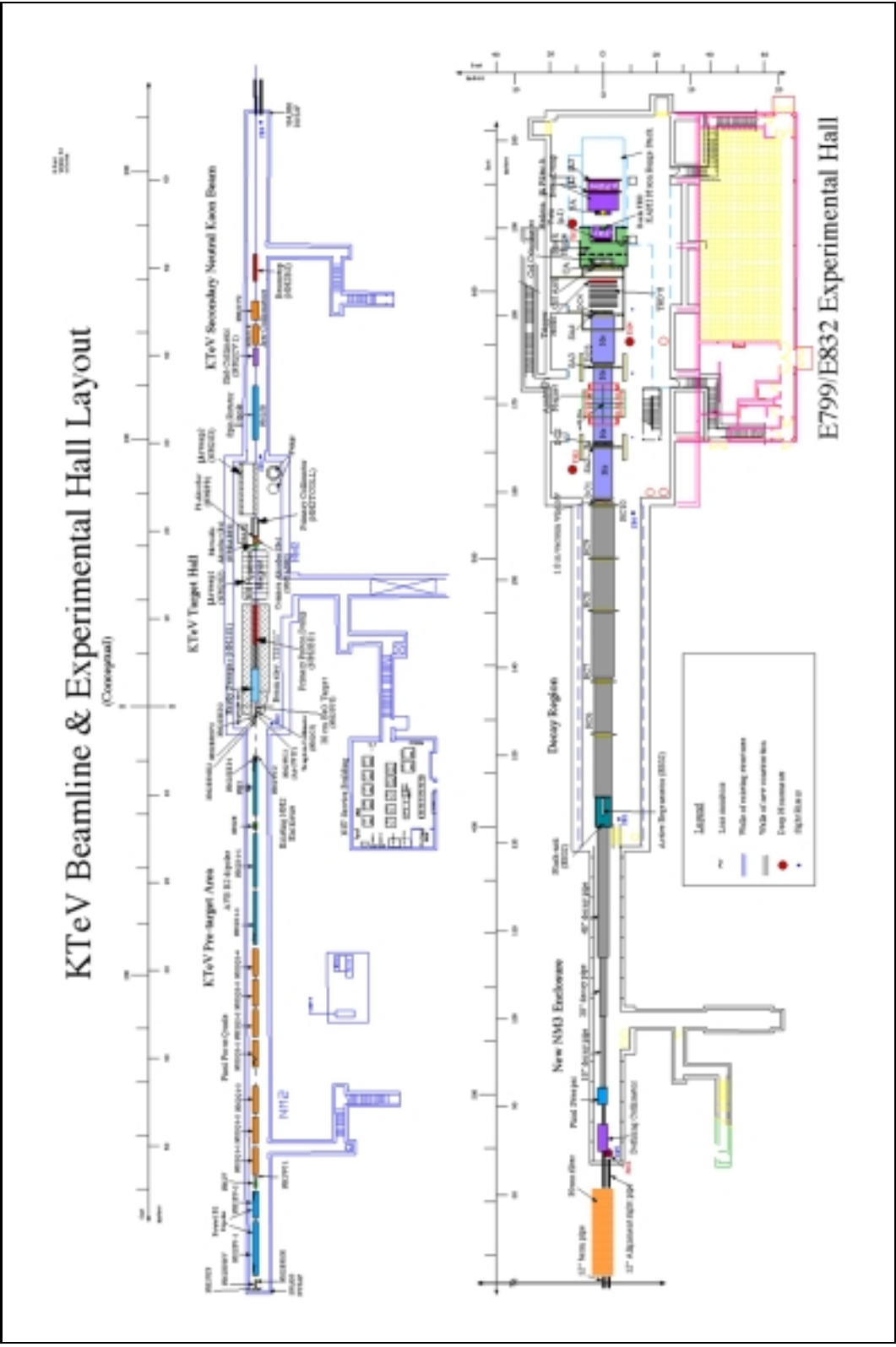


Fig. 3. KTeV experiment layout

2. Primary Proton Beam

2.1 *Layout and tunnel constraints*

For the KTeV beamline, only modifications in enclosures NM1 and NM2 were needed. The modifications in enclosure NM1 were minor. The KTeV primary beamline as designed is able to run up to 900 GeV though the actual operating energy was 800 GeV.

Figure 4 shows the magnet layout in enclosure NM2. Three conflicting issues had to be resolved: a) to increase the target height to allow for shielding under the target for ground water considerations, the up bend in NM2 should be as far upstream as possible and the down bend as far downstream as feasible (also needed is an east bend to match the existing enclosure downstream of the target); b) to increase the accuracy of beam position and slope measurement, one position measuring device should be very close to the target and another one as far upstream as possible; and c) to maximize its range, the Angle Varying Bend (AVB) system needs to be close to the target. The conflict is resolved as follows.

At the upstream end, after leaving about 2 m for instrumentation, the beam is bent east and up by NM2EU, a string of two B2 dipoles rotated 30.4 degrees. A vertical trim (NM2V) follows NM2EU, allowing for independent adjustment in the horizontal and vertical planes. At the downstream end, a pair of position measuring devices (NM2WC3, NM2SEED2) are located 0.6 m upstream of the target, and a second pair (NM2WC2, NM2SEED1) about 5 m upstream of the previous pair—this allows extrapolation to the target with minimal loss in position resolution. The redundancy was required because the SEEDs were new devices which were not guaranteed to be working at startup. The AVB system (NM2D1/NM2D2) is placed upstream of NM2WC2 (the horizontal trim NM2H is inserted here for fine control). The final focusing quadrupoles (NM2Q1/NM2Q2) are placed in the remaining space, between NM2EU and the AVB system. The KTeV primary beam position at the target is eleven inches higher than the original beamline elevation.

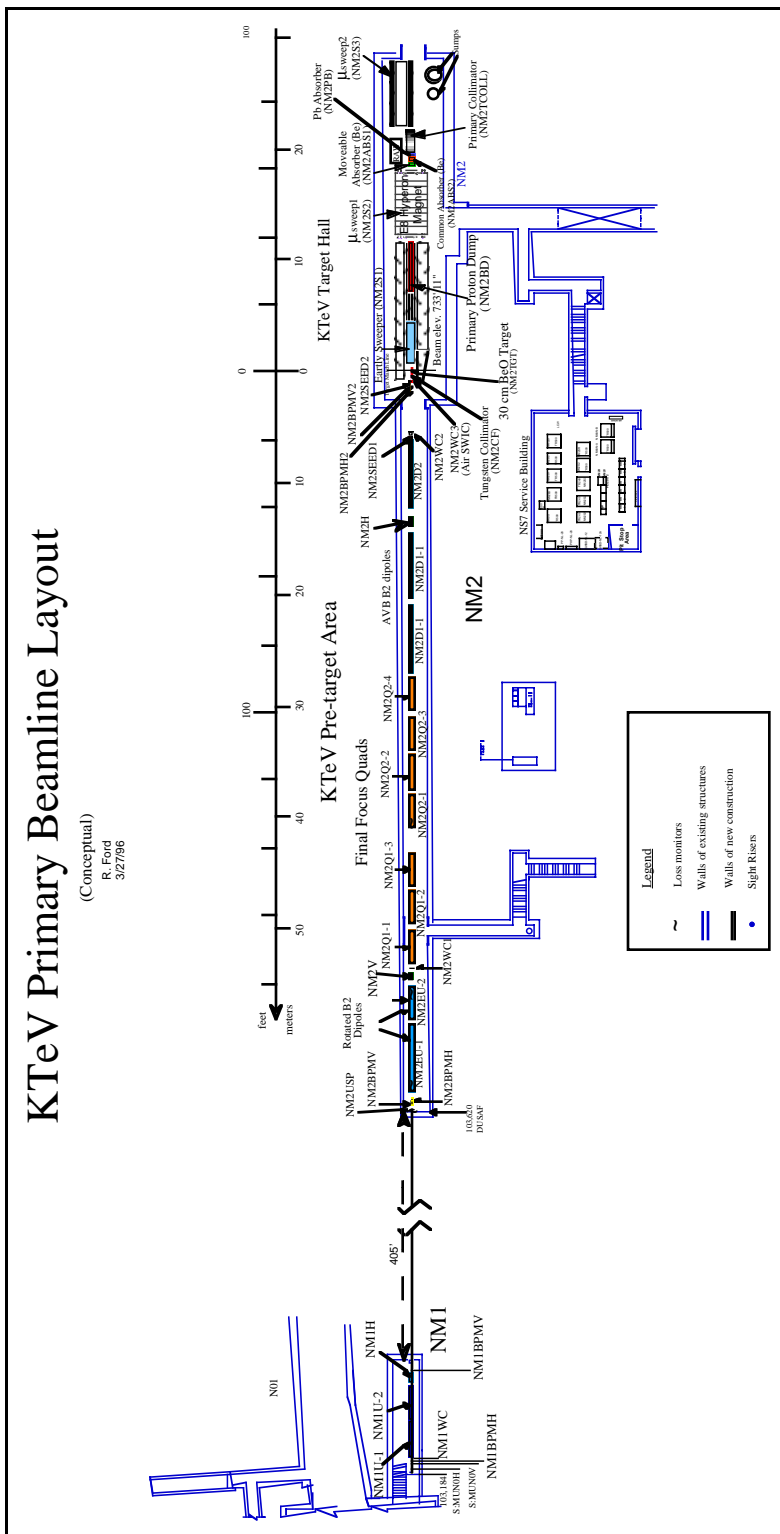


Fig. 4. Layout of primary beam components in NM1 & NM2

This gain in elevation was achieved by positioning the beam two inches away from the top of the NM1 to NM2 pipe and by bending the beam up with NM2EU and back down with NM2D1 and NM2D2.

2.2 The Angle Varying Bend (AVB) system

The vertical targeting angle can be changed using NM2D1 and NM2D2. Figure 5 shows a picture of the AVB system. The thicker line is the -4.0 mrad beam trajectory; the thinner line is the -5.6 mrad trajectory.

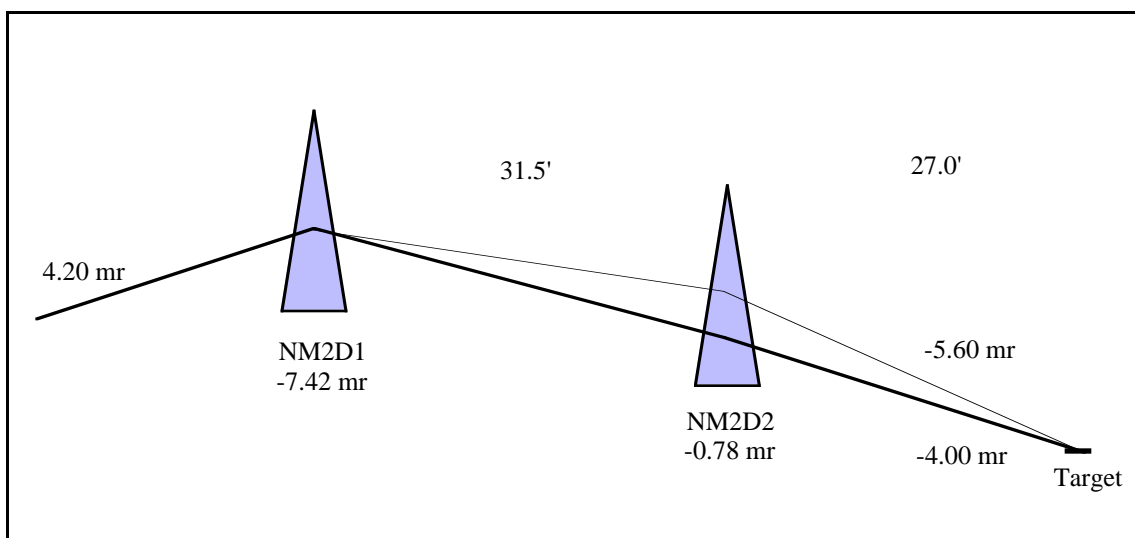


Fig. 5. AVB system layout. The vertical and horizontal scales are different.

As can be seen in the figure, the angle is the smallest when NM2D2 is at its lowest field value. By increasing the NM2D2 field and at the same time decreasing NM2D1, the angle can be increased without changing the beam position at the target. The targeting angle is maximum when NM2D2 reaches its maximum. The bigger the NM2D2 range, the bigger the range in targeting angle. A range of 0 to 4800 amps was assumed for NM2D2 (a B2 magnet).

The beam is rising in front of the NM2D1 magnets. The NM2D1 and NM2D2 magnets are used to bend the beam down. At 900 GeV/c, the two B2s in the NM2D1 string are not enough to bend the beam down to the minimum angle required (-4.0 mrad); therefore, the minimum value of NM2D2 must be greater than zero. If the

minimum current of NM2D2 were to be reduced to zero, then the range of the AVB system would increase by 20%.

During the run, it was discovered that due to substation load, NM2D2 could not ramp up much over 4400 amps. This reduced the maximum targeting angle to 5.4 mrad. Also, uncertainties in the actual current of the AVB magnets necessitated the use of the SEEDs in setting the precise currents for each targeting angle.

2.3 Instrumentation

Most of the instrumentation used was standard devices found throughout the Fermilab external proton beamlines. These devices include Segmented Wire Ionization Chambers (SWICS), split-plate rf pickups (BPMs), and gas ionization chambers or "loss monitors". Their locations are indicated in fig. 4.

For the region near the target, very good position resolution and the ability to accurately measure beam profiles were needed. For this application a new Secondary Emission Electron Detector (SEED) was developed⁵. The beam positions from the SEEDs and other beamline instrumentation were used by an automated beam tuning program described in Section 2.5 (AUTOTUNE). The wire spacing in the SEEDs was 125 to 250 microns. SEED profiles of the primary beam at the target are shown in fig. 6.

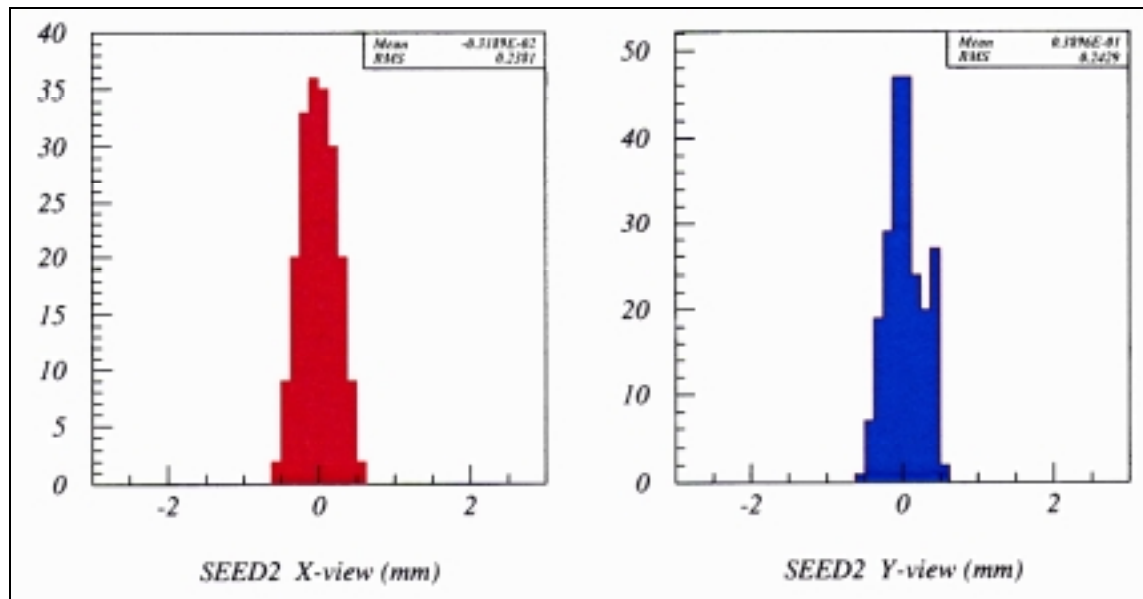


Fig. 6. Horizontal and vertical beam profiles at the target with noise cut. The “hot” wire on the right side of the vertical profile was present throughout the run and was very stable. AUTOTUNE was offset by 0.05 mm to compensate for it. The wire will be examined to determine the cause.

The target SEED was tested for signal degradation since it had the highest integrated flux density and the beam was focused on the same spot for the entire run. The signal strength was tested by moving the beam to various locations on the wire and comparing the integrated signal. The result was a 20% drop in signal strength for a one year run of $\sim 3 \times 10^{12}$ ppp and a beam sigma of $240 \mu\text{m}$ or 2.2×10^{21} protons/cm². This was not a problem since this SEED was not used for intensity monitoring. Figure 7 illustrates the resolution of the target SEED. In order to test the resolution, the beam was moved up and down an equal amount by changing a magnet current. This was done on alternating spills to eliminate any effects of beam drift. Each point represents the average beam position of 9 samples during an 18 second spill interval with random readout noise subtracted. The plot shows that at each of the two magnet settings, the beam and SEED are stable within about $10 \mu\text{m}$ over the period tested with an estimated $2 \mu\text{m}$ beam drift.

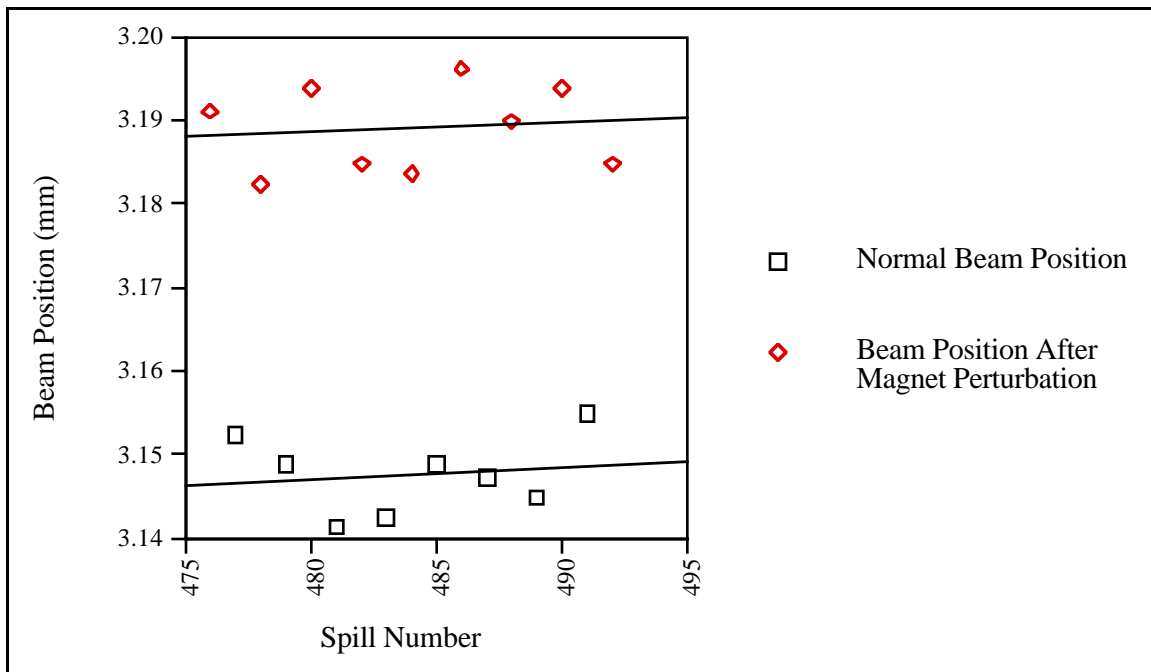


Fig. 7. KTeV target SEED resolution & beam stability

Two SWICs and the target SEED were used for position and angle monitoring as feedback inputs for AUTOTUNE. New BPMs and a new digital electronics readout were made for KTeV and were intended to give a non-interactive beam position input for AUTOTUNE. An as yet unresolved problem with the new BPM digital electronics produced stability problems which precluded their use with AUTOTUNE or for intensity monitoring.

For the first half of the 1996/97 run, intensity was monitored using a standard SEM and a Switchyard BPM as a back-up. The Switchyard BPMs utilize the original analog electronics design. However, starting in April 1997, the BPM INH424 became the official intensity monitor using the other switchyard BPMs as backup. This eliminated the calibration problems associated with loss of secondary emission efficiency and also reduced the radiation backgrounds in NM2. The recorded integrated proton flux for the 1996/97 fixed target run⁶ was 7.0×10^{17} , with 1.6×10^{17} recorded for calendar year 1996 and 5.4×10^{17} for 1997.

2.4 Optics/spot size at target

The three goals that guided the design of the primary beam optics were:

- To achieve the requested beam size.
- To form a beam waist at the target.
- To minimize the dispersion at the target.

The requested beam size is $\sigma \leq 250 \mu\text{m}$ for both the horizontal and vertical beam profiles. A waist at the target will provide: a) minimum beam size change through the target, and b) beam size stability. Since the beam coming out of the Tevatron is not monochromatic, to achieve maximum position and angle stability the dispersion at the target needs to be minimized. The optics is discussed in detail elsewhere⁴. The spot size at the target as shown in fig. 6 is slightly less than the specification of sigma <250 microns in both planes.

2.5 AUTOTUNE

AUTOTUNE⁷ was implemented in the fall of 1996 in order to provide position and angle stability on the target. In order for this system to function for long periods of time in automatic mode with no human intervention, it was kept as simple as possible using only three feedback inputs. It was also important to make transport constants as accurate as possible. In order to compensate for uncertainties in magnet currents, fields, and positions, transport constants were modified based on actual current versus position measurements. This technique worked quite well for the entire run with the only minor problems arising from keeping the computer process running and saving the appropriate markers on the SWIC scanners.

With the regular settings of NM2Q1 at 730.6 amps and NM2Q2 at -746 amps the relationship between changes in the magnets' fields and beam positions is given by (the units are mm/kGauss):

		NM0H	NM0V	NM1U	NM1H	NM2EU	NM2V	NM2H	NM2D2
NM1WC	H	28.15	0.00	0.00	0.00	0.00	0.00	0.00	0.00
NM1WC	V	0.00	8.96	0.00	0.00	0.00	0.00	0.00	0.00
NM2WC1	H	44.74	0.00	0.00	3.94	1.92	0.00	0.00	0.00
NM2WC1	V	0.00	14.49	32.40	0.00	1.19	0.03	0.00	0.00
NM2SEED1	H	2.50	0.00	0.00	1.55	20.79	0.00	0.22	0.00
NM2SEED1	V	0.00	5.58	15.41	0.00	4.11	0.59	0.00	0.79
NM2SEED2	H	-0.17	0.00	0.01	1.50	23.47	0.00	0.36	0.00
NM2SEED2	V	0.00	2.02	7.39	0.00	3.73	0.57	0.00	1.90

With the above matrix it is possible to study the accuracy that is needed in the beam position measurements to achieve a 50 μm and 20 μrad beam stability at the target. These goals are slightly better than the design specifications of 100 μm and 25 μrad .

Horizontal stability

It would be preferable to use only NM0H and NM1H to control the horizontal, but this would require better position resolution than possible with NM2WC1 (130 μm). Therefore NM2EU must be used. As NM2WC1 is so close to NM2EU, the constants from NM2SEED1 and NM2SEED2 must be used to calculate the slope resolution. Since the distance between NM2SEED1 and NM2SEED2 is 5 meters, the error in the slope is given by

$$\begin{aligned}\sigma_{\theta}^H &= \sqrt{\left[\left(\frac{2.5 + 0.17}{28.15 \times 5000} \times 10^6 \right) \sigma_{NM1WC}^H \right]^2 + \left[\left(\frac{1.55 - 1.50}{3.94 \times 5000} \times 10^6 \right) \sigma_{NM2WC1}^H \right]^2} \\ &= \sqrt{(19 \sigma_{NM1WC}^H)^2 + (2.5 \sigma_{NM2WC1}^H)^2} \quad \mu\text{radians}\end{aligned}$$

Therefore a 1 mm accuracy in the position measurements will be enough to achieve a 20 μrad angular stability.

The calculations show that NM2EU has to be included to control the beam position at the target. The minimum step size in NM2EU is 0.183 amps, which reflects a change of 12 μm at NM2SEED2, so the resolution in the current is there. The error in the slope introduced by using NM2EU will be:

$$\begin{aligned}\Delta\theta_H &= \frac{\Delta x_{NM2SEED2} - \Delta x_{NM2SEED1}}{5000} \times 10^6 \\ &= \frac{1 - 0.886}{5000} \times 10^6 \Delta x_{NM2SEED2} = 23 \Delta x_{NM2SEED2}\end{aligned}$$

So a change of 0.050 mm in NM2SEED2 produces a change of 1 μ rad in the slope. Therefore the best solution for the horizontal control is to use the magnets NM0H, NM1H, NM2EU, the monitors NM1WC, NM2WC1, NM2SEED2, and to require an accuracy in the beam position in each SWIC of 1 mm, 1 mm and 0.050 mm respectively.

Vertical stability

To achieve a vertical stability of 50 μ m, NM2V and NM2SEED2 will have to be used. NM2V has the capability of making changes at NM2SEED2 producing only small changes in the angle. The error in the angle coming from the use of NM2V is:

$$\Delta\theta_V = \frac{1 - 1.035}{5000} \times 10^6 \Delta y_{NM2SEED2} = -7 \Delta y_{NM2SEED2}$$

which gives an error of 0.35 μ rad when the beam is moved at NM2SEED2 by 50 μ m.

Therefore the best solution for the vertical control is to use the magnets NM0V, NM1U, NM2V, the monitors NM1WC, NM2WC1, NM2SEED2, and to require an accuracy in the beam position in each SWIC of 1 mm, 1 mm and 0.050 mm respectively.

2.6 Primary beam stability results

KTeV requires $\leq \pm 100$ μ m beam position stability (horizontal and vertical) with an angular stability of $\leq \pm 25$ microradians. The new SEEDs were designed to have resolution such that this stability is measurable. The program AUTOTUNE was developed to maintain this stability. By looking at data we see that the stability required was both achieved and maintained⁸.

Each SWIC or SEED may be set to sample data from one to ten times during each spill. In this case, the SEED was set for ten scans; scan five was used to calculate pulse-to-pulse stability because it is used in AUTOTUNE. Stability during the spill was calculated by taking the difference between scan ten and scan three.

Figures 8a and 8b show the vertical and horizontal beam position for scan five as a function of time. The vertical line at day six is when autotuning began. It is evident from the graphs that long-term stability has improved since AUTOTUNE was implemented. Two possible exceptions are during day 15, when there were problems with power supply regulation, and a short period on day 16.

Figures 8c-f show average positions, summed over the collected data, both before and after AUTOTUNE was implemented. In both, the RMS has decreased, and the distribution approaches a Gaussian shape. From these histograms the beam stability may be calculated by multiplying the RMS by the wire spacing.

Recalling that NM2SEED2 has a 125 μm wire spacing, we summarize the stability in Table 3:

Table 3. Stability before and after implementation of AUTOTUNE.

NM2SEED2	Before	After	Improvement
Vertical	71.9 μm	54.8 μm	17.1 μm
Horizontal	83.4 μm	56.5 μm	26.9 μm

Finally, stability during the spill (“beam roll”) may be examined. Figures 9a and b show the difference in the average vertical and horizontal positions for scans ten and three. The horizontal line in each graph is at zero. We see that horizontally the beam does not roll by more than about one wire (125 μm). Vertically, the roll was quite dramatic until day 13, when a faulty power supply was repaired. The “scatter” between days 14 and 16 is also due to regulation problems. Figures 9c-f show the vertical and horizontal beam roll before and after day 13 (left and right columns, respectively).

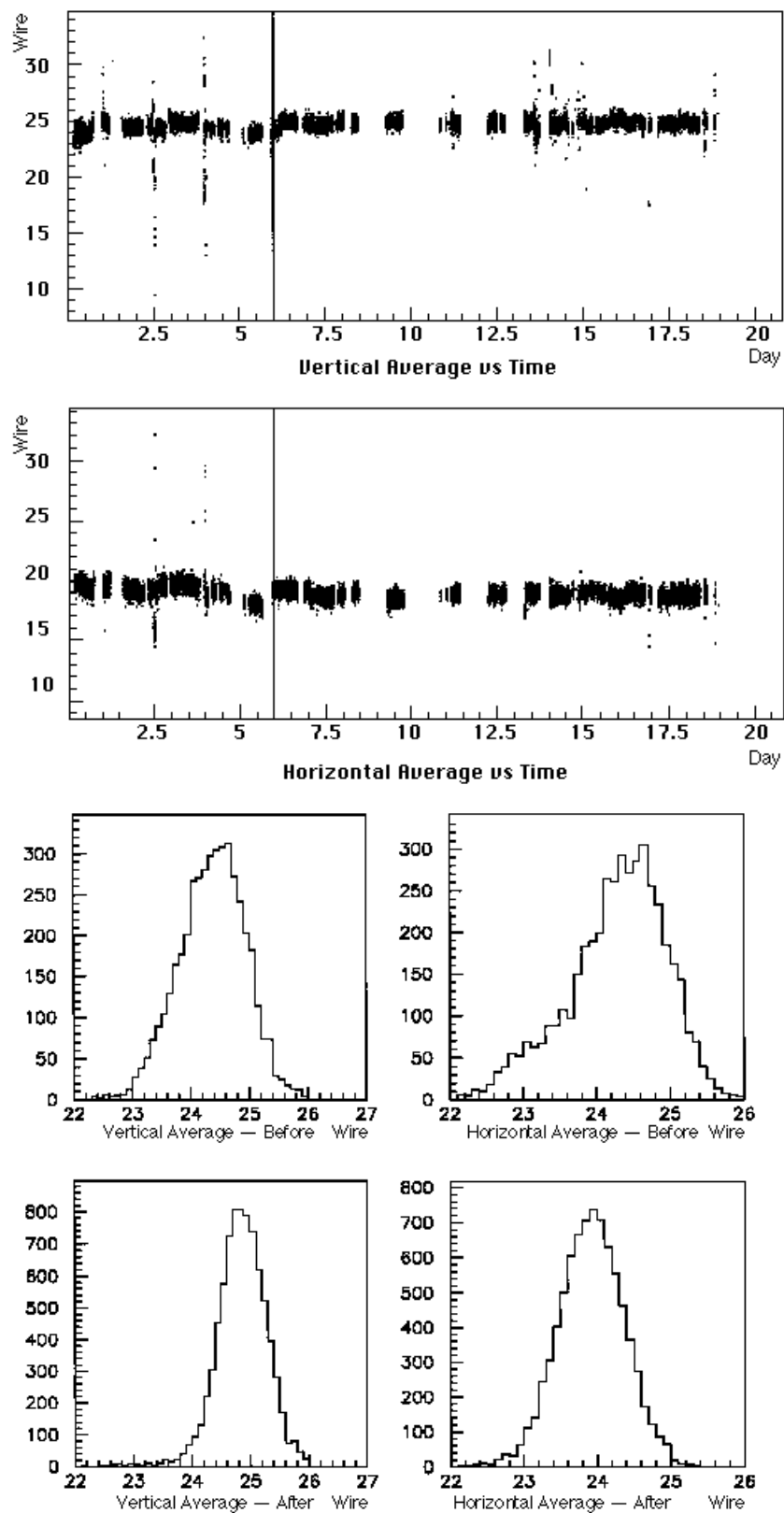


Fig. 8a-f. Primary beam position for scan 5 and histograms before and after AUTOTUNE implementation. Wire spacing is 125 microns.

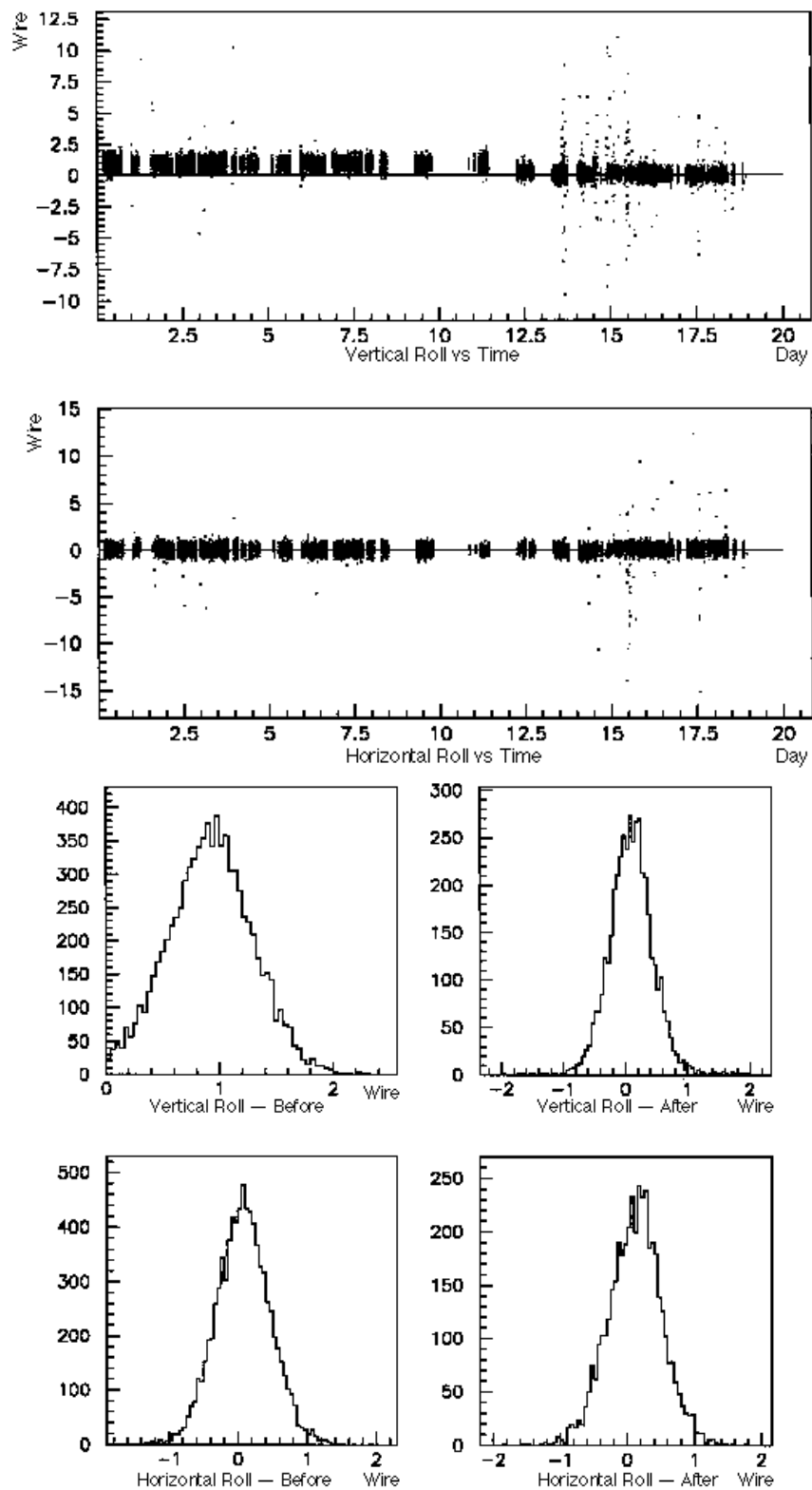


Fig. 9a-f. "Beam Roll" (difference of beam position between scan 10 and scan 3). Histograms of same before and after power supply regulation problems. Wire spacing is 125 microns.

The results are summarized in Table 4 below:

Table 4. Beam roll before and after day 13.

NM2SEED2	Before	After
Vertical	115 μm	12.7 μm
Horizontal	9.19 μm	11.3 μm

Another study was done in February (KTeV run #8384) which does show some beam roll during the spill in the horizontal plane (see fig. 10). The cause and frequency of this is still under investigation. The current AUTOTUNE program only compensates for long term beam changes, not intraspill beam roll.

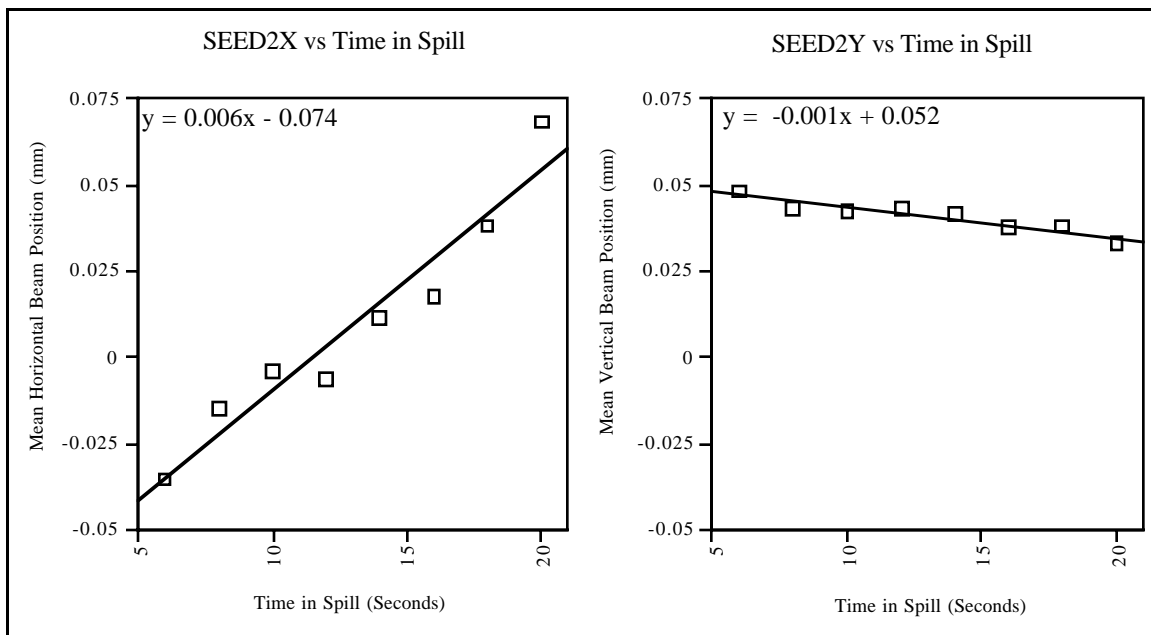


Fig. 10. Mean beam position on SEED2 as a function of time in spill for KTeV run #8384 (~440 spills). The first two scans are not shown (little or no beam due to E815 pings).

One last illustration of the primary beam stability is the visible spot from radiation damage on the Kapton window of the target SWIC NM2WC3 shown in fig. 11.

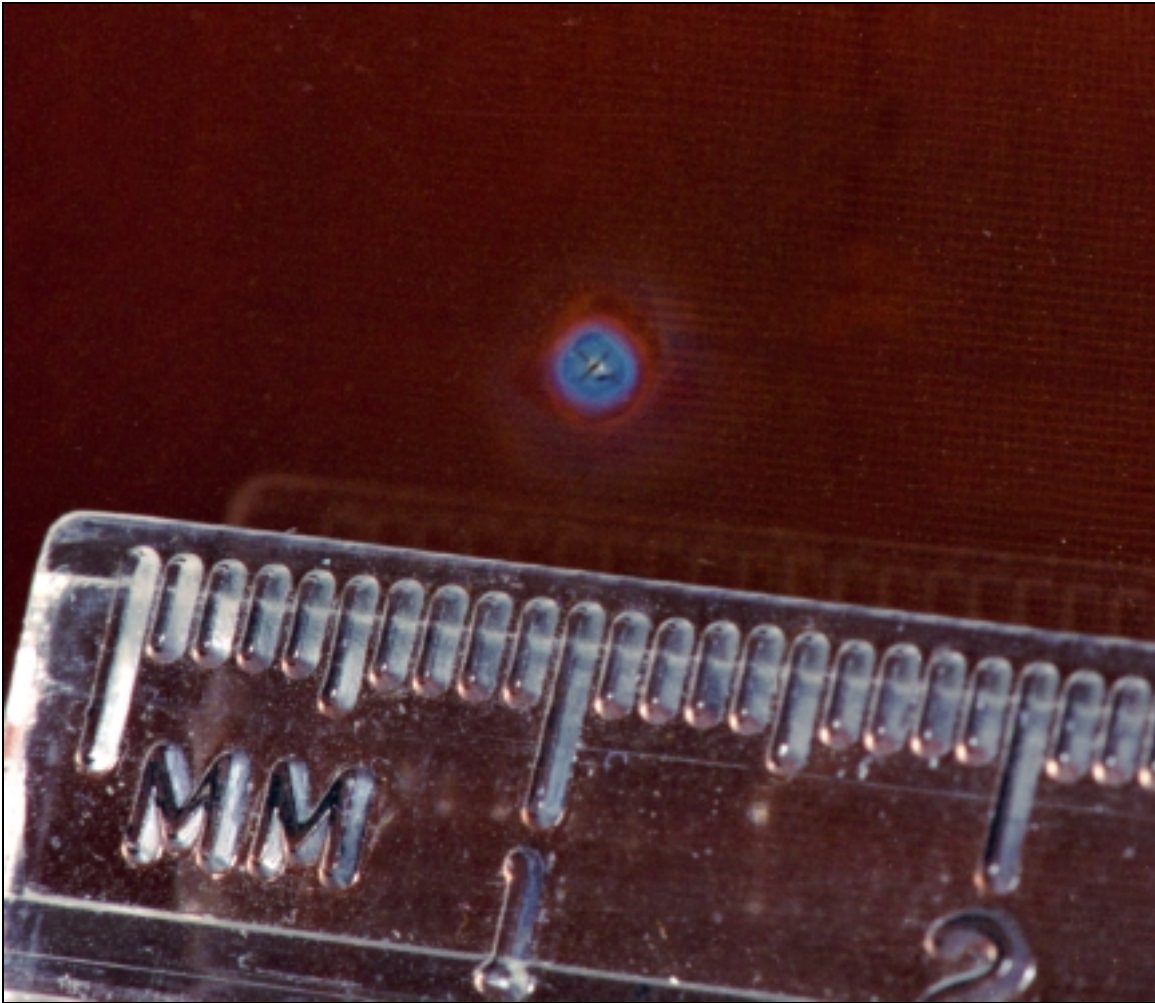


Fig. 11. Photograph of burn mark on Kapton window of NM2WC3 located in front of the primary target. This mark gives visual evidence of the size, location, and stability of the KTeV primary beam. The outer ring measures 1.4 mm and the inner ring measures 0.76 mm.

In conclusion, the spill-to-spill stability of the beam is better than $60\ \mu\text{m}$. Implementing the AUTOTUNE program has improved this stability. “Beam roll” (or motion of the beam at the target during the spill) varies in magnitude over time during the year of running. Elimination of this source of error is not possible with the current controls system, but should be eliminated with future control system upgrades.

3. Target Station and Muon Sweeping System

3.1 Overview

The Target Pile System was designed to:

- produce neutral kaons
- sweep unwanted charged particles out of the NM2 acceptance
- sweep muons beyond the acceptance of the experiments
- absorb the primary beam that does not interact in the target
- provide Beam-On shielding
- provide Beam-Off, personnel access shielding
- provide groundwater protection
- provide cooling

The items and subsystems that performed these tasks are:

- the target, target drives and maintenance platform
- the NM2S1, NM2S2 and NM2S3 sweeping magnets
- the NM2 primary beam absorber, NM2BD
- steel shielding
- the LCW and RAW cooling systems

These systems are described in detail in the KTeV Beam Systems Design Report⁴, but brief descriptions and performance notes follow.

3.2 Muon sweeping system

Muon and charged particle sweeping after the target was performed by three dipole magnets NM2S1, NM2S2 and NM2S3. While each magnet has a unique design, together they sweep charged particles out of the subsequent NM2 beamline apertures and sweep muons outside of the acceptance of the KTeV experiments. All three magnets are operated with the same sign central field and all sweep in the horizontal plane.

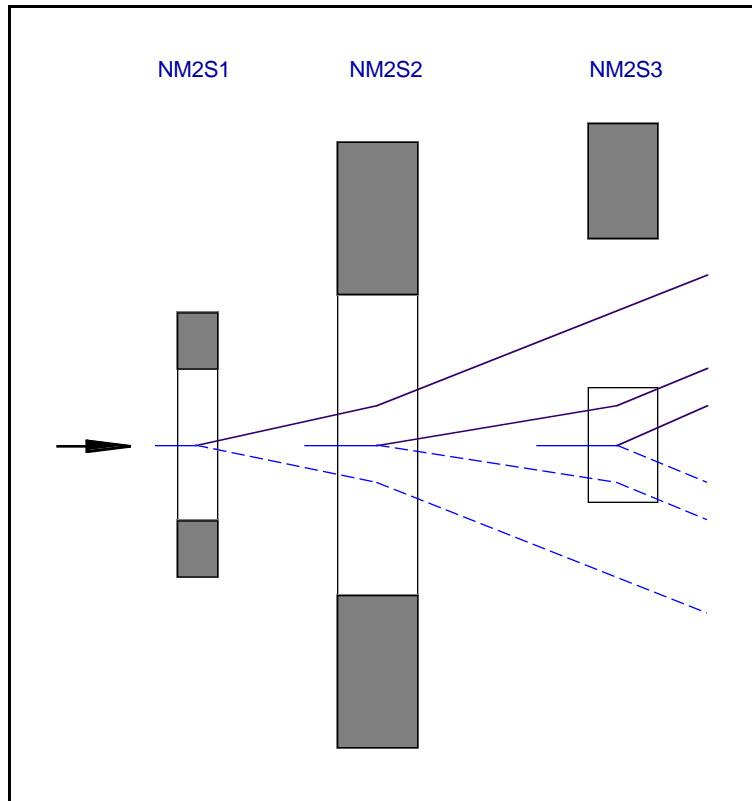


Fig. 12. Muon sweeping system

In fig. 12, the white rectangles indicate the same-sign central magnetic fields and the gray the return yokes. The bulk of the muon distribution lies within the same-sign pole-face regions and within the field free region of NM2S3. All magnets sweep in the horizontal plane, positives (solid lines), towards the west. NM2S1 is a standard Fermilab external beams target sweeper dipole, also referred to as an Eartly magnet. It was regapped from 1.125" to 2.50" and has a maximum field of 9 kG. NM2S2 is a large dipole previously used in the Fermilab E8 Hyperon experiment, regapped for our purposes⁴. Finally NM2S3 is a new magnet designed and built for this beam. NM2S3 is a "C-type" magnet with the return yoke displaced to avoid the main muon plume as shown in fig. 12. It has a maximum field of 19 kG. NM2S3, in addition to muon sweeping, also provides cleanup sweeping in the neutral channel for products from interactions in the lead and beryllium absorbers just upstream of it.

The muon sweeping function of these three magnets results in two horizontal "lobes" of muons of opposite sign, the centroids of

which lie outside of the acceptance of the detector. During normal data-taking conditions the positions of the lobes lie outside of the detector by design. However a special run in which the magnetic fields were decreased shows two, partially collapsed, horizontally opposed lobes within the acceptance of the muon counters⁹ (see fig. 13).

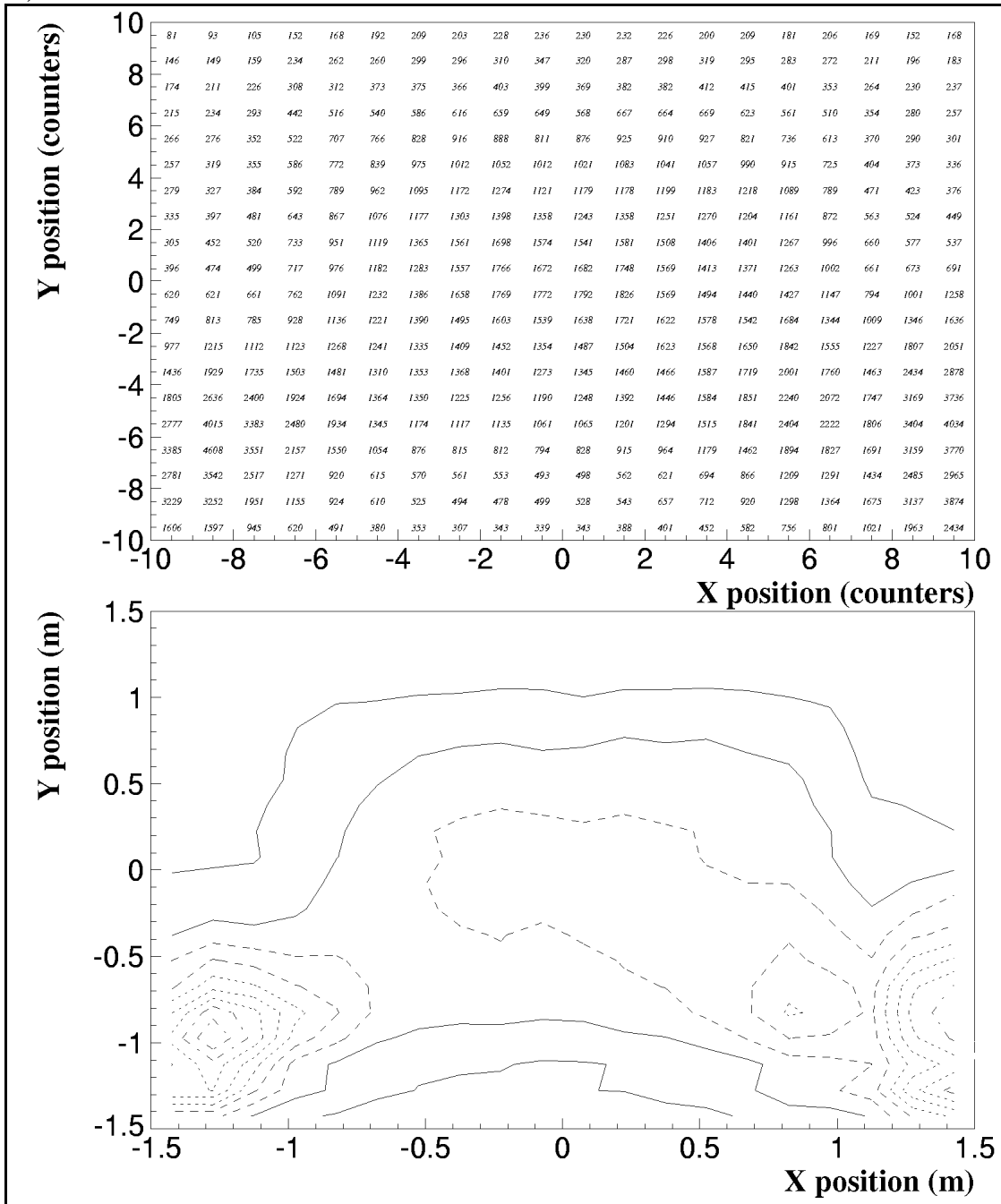


Fig. 13 a and b. Muon distribution during special run

The sweeper currents are given in Table 5. The value of NM2S3 was set at 875 (320) amps so that the lambda (cascade) particle's polarization was rotated by 270 degrees from all three sweepers (see Section 4.9). The initial interest of the KTeV hyperon group shifted from the lambda particle to the cascade particle with the first observation of the cascade beta decay. As we will see in the next section this reduction of NM2S3's current does not effect the muon rate in the detector significantly.

Table 5. Predicted and actual operating currents (fields) of the muon sweeping system magnets.

	NM2S1		NM2S2		NM2S3	
	I(amps)	B(kG)	I(amps)	B(kG)	I(amps)	B(kG)
E832 Operation	550	4.3	1500	23	875	18
E799 Operation	550	4.3	1500	23	320	12
Special low field study	550	4.3	1500	23	0	0

3.3 Measured muon rates in KTeV from the target station

There are several sources of muons as measured by the KTeV detector. Muons can originate in the target station from the primary beam striking the production target or beam dump. Muons can also originate from kaon decays along the neutral beam and neutral beam interactions in the detector. The target station source can be isolated from other sources by inserting the NM2BS beam stop into the neutral beam. This absorbs the neutral beam in iron block far upstream in the beamline, leaving the target station muons as the dominant source. The goal for the target station muons was less than 100 kHz for 5×10^{12} protons on target. This is motivated by the ~40 (200) kHz rate from kaon decays in the KTeV detector decay region during E832 (E799) running conditions.

The target station muon rate in the experiment normalized to the primary beam intensity is plotted versus current in NM2S2 and NM2S3 in fig. 14. The result is 60 kHz for 5×10^{12} protons on target well below the 100 kHz goal.

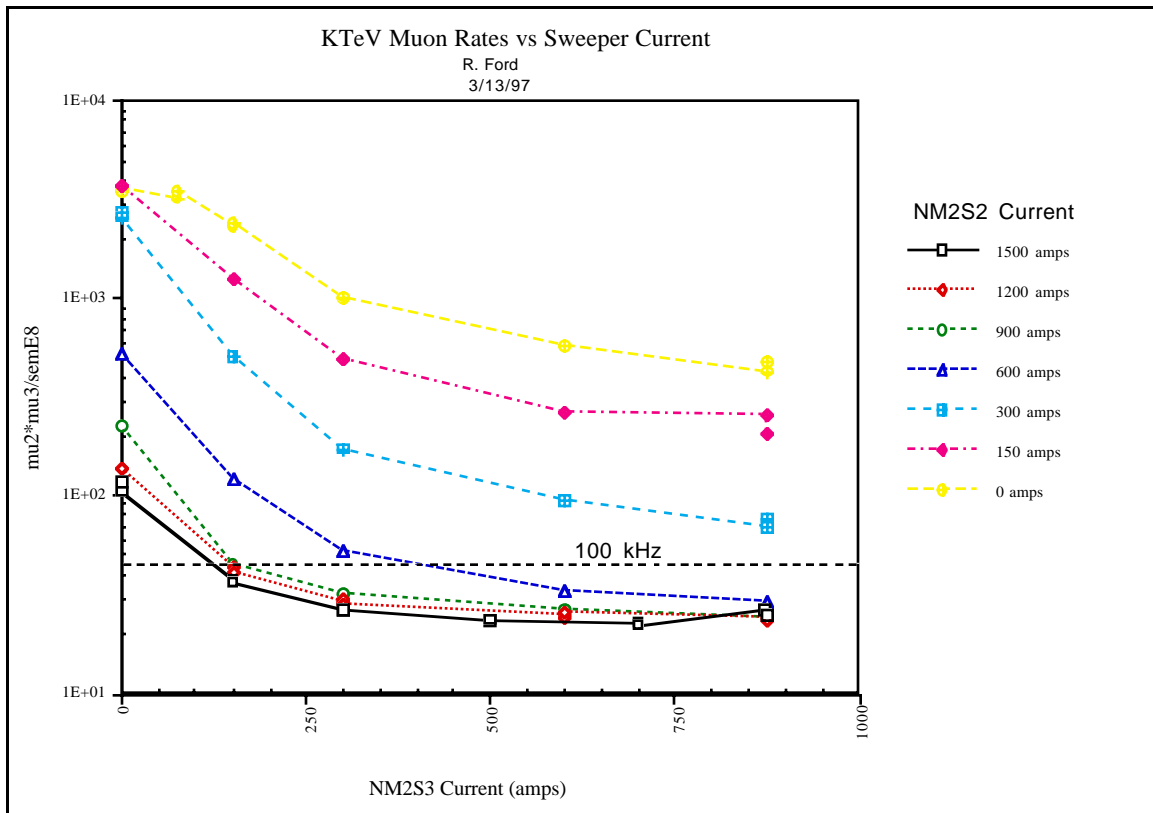


Fig. 14. Muon rates vs NM2S2 and NM2S3 currents

3.4 Shielding

Measurements made of the residual radioactivity on the outside surface of the target pile indicate a maximum of 10 mrem/hour at 1 foot, 16 hours after turn-off¹⁰ and 50 mrem/hour at 1 foot, 1/2 hour after turn-off¹¹. Both are well within the 100 mrem/hour at 1 foot guideline.

The Single Resident Well groundwater model was used to estimate the production of H³ and Na²². This model suggests that for 2×10^{18} protons per calendar year, the ratio of allowed concentrations of H³ and Na²² is 0.08 and 0.05 respectively. The table below summarizes the expected H³ and Na²² concentrations based on the actual intensity⁶ for each calendar year that the experiments operated.

Table 6. Ratio of expected to allowable radionuclide production in the groundwater surrounding NM2

	Calculated Intensity	1996 Integrated Intensity	1997 Integrated Intensity
	2×10^{18}	1.59×10^{17}	5.43×10^{17}
H ³	0.08	0.006	0.022
Na ²²	0.05	0.004	0.014

3.5 Cooling

The supply and the return of the Radioactive Water (RAW) cooling system were at equilibrium with each other and operated at a fairly constant 5 F° above the Low Conductivity Water (LCW) system that provides cooling to the RAW. This suggests that the 60 gallon RAW system is sufficient to provide cooling for the heat loads represented by NM2S1, the NM2S2 inserts, the NM2 primary beam absorber and of course the beam.

4. Secondary Neutral Beam

4.1 *Layout and overview*

The neutral beam target/collimation scheme must produce the required kaon flux within a solid angle small enough with respect to the beam holes through the CsI calorimeter such that radiation damage and excess activity in the CsI is minimized. This means careful control of collimator machining and overall system alignment. Tails on the neutral beam shape due to absorber scattering must be minimized. Trigger rates in the experiment are also much lower in a halo-free clean neutral beam. Finally, material in the beam region of the detector must be as low as practically achievable which is particularly important for low trigger rates. The physics requirements of the E832 CP violation studies also demanded precisely matched neutral beams of equal size and kaon momentum distributions with excellent stability.

The 800 GeV primary proton beam strikes a 30 cm BeO target with a downward angle of 4.8 mrad with respect to the neutral channel. The target's alignment is remotely adjustable. The rate of interactions in the target is monitored by a scintillation counter telescope located at 90 degrees to the primary beam. These counters "view" the target through a 1/4"x1/4" hole in the 4 ft thick iron shield approximately 6 ft transversely from the target location and near the mid-point of the target length. The counting rate of a 3-fold coincidence is approximately $\sim 10^{-6}$ of the incident proton intensity. The 4.8 mrad angle improves the kaon to neutron ratio by an order of magnitude compared to zero degree targeting. The loss of kaon flux is about a factor of three relative to zero degrees.

The magnetic sweeping required for muon reduction is more than enough to eliminate charged particles from the neutral channel. The proton beam which does not interact in the primary target is absorbed on the beam dump located in the region with the large iron shield for radiation safety protection. Apertures in the heavily shielded target station are over-sized relative to the final neutral

beam solid angle, thus avoiding tight alignment tolerance in a high radiation area. Similarly the apertures in the large dipoles (NM2S2,3) are over-sized also. (see Section 3 for a discussion of muon sweeping and beam dump).

Photons dominate the neutral flux after NM2S2. To eliminate the photons, 3" of Pb is placed in the beam at this point. The remaining neutron flux is still several times larger than the neutral kaon flux. So just upstream of the Pb absorber we place beryllium in the beam also. Beryllium enhances the kaon to neutron ratio. Beryllium is also used to attenuate the E832 beam which strikes the regenerator. The lengths and attenuation from the various absorbers are shown in Table 7.

Immediately following the absorbers is the primary collimator which serves to provide initial collimation. The primary collimator is designed to have sufficient shielding for the amount of neutral beam dumped in this region. The collimator is remotely adjustable. This collimator also plays an important role in limiting the size of the source at the absorbers thus minimizing tails on the beam at the CsI holes.

Continuous vacuum begins just upstream of NM2S3. After NM2S3, the rotator dipole is used to rotate the hyperon polarization (see Section 4.9). The slab collimator is a 10 ft long block of steel which is positioned between the two neutral beams to prevent an absorber scatter in one beam from crossing over into the other beam. The two "jaw collimators" are a pair of 5' (7') long iron blocks which close on the horizontal (vertical) outer edges of the beam. These serve the purpose of varying the beam size for special studies and also could, in principle, provide some reduction of the flux on the following defining collimator. In practice these were very useful for special studies, but were not used for reducing the flux on the following collimator. The neutral beam then passes through a 12" diameter vacuum pipe surrounded by a steel muon shield, before reaching the defining collimator in the next enclosure.

The defining collimator makes the final cut on the neutral beam. The position and alignment of this collimator is remotely adjustable.

4.2 *Design of neutral beam collimation scheme*

The arrangement of the collimator scheme was first worked out in the KTeV Design Report¹. The principal concern was to prevent a single elastic scattering in the absorbers from hitting the CsI calorimeter. Analytic equations were derived to specify the maximal absorber scattering ray at the CsI. In addition, care was taken in the taper of collimators, including finite target size effects, to minimize backgrounds from interactions in the collimators. The location of the upstream collimator is largely determined by the amount of space needed to dump the protons which do not interact in the target and the initial muon sweeping. The absorbers were placed as far upstream as accessible. The primary collimator was located immediately downstream of the absorbers.

The defining collimator was located as far downstream as possible to minimize motion of the neutral beam correlated with motion of the primary beam on target. Past experience, in experiments in Meson Center, indicated that the backgrounds were small even with the final defining collimator at $z = 85$ m from the target with the CsI located at 186m. The maximal scattered ray was chosen to be well within the CsI beam hole (1 cm away from the 15 cm CsI beam hole, 9.3 cm x 9.3 cm beam size).

After this initial design work, more detailed studies based on GEANT⁴ followed. These studies predicted the radiation damage expected with the above design criteria as well as the expected trigger rates (see Section 4.7).

4.3 *Particle fluxes*

Particle fluxes are based on our previous measurements in the Meson Center beamline at Fermilab² with the exception of the cascade which used parameterizations of Pondrom et al¹².

Table 7. Predicted neutral fluxes

	E832 regenerator	E832 vacuum	E799 both beams
incident protons	3.5×10^{12}	3.5×10^{12}	5.0×10^{12}
K_L^0	3.5×10^7	1.4×10^7	2.9×10^8
neutron	7.0×10^7	2.2×10^7	1.1×10^9
lambda	1.7×10^4	5.2×10^3	2.6×10^5
cascade	9.1×10^2	2.8×10^2	1.4×10^4
filters	3" Pb + 20" Be	3" Pb + 38" Be	3" Pb
K_L^0 transmission	.19	.076	.55
n transmission	.10	.031	.54

Neutral fluxes shown are at $z = 90$ m from the target per spill (solid angle = 0.25 mster. per beam). The transmission includes the effect of absorption and scattering from the filters. The transmission for lambda and cascade were taken to be the same as the neutron.

Table 8 compares the predicted fluxes from Table 7 with the preliminary results on flux measurements. The E799 K_L^0 fluxes are determined from comparing 8 different K_L^0 decay modes¹³ which are consistent to $\pm 5\%$. The absolute normalization is known to about 15% limited by our beam intensity calibration. The neutron rate is estimated from the E832 regenerator rate after subtracting the rate due to the known K_L^0 flux. Finally the hyperon fluxes are based on preliminary results from the E799 hyperon group analysis¹⁴.

Table 8. Measured fluxes vs predicted

Particle Type/Condition	Measured Flux	Ratio Measured/ Predicted
K_L^0 E799 both beams	2.1×10^8	0.7
neutron / E832 vacuum	8.4×10^7	1.2
lambda / E799 both beams	3.1×10^5	1.2
cascade / E799 both beams	1.5×10^4	1.1

4.4 Energy spectrum of neutral kaons

The energy spectrum observed in KTeV during E832 for $K_L^0 \rightarrow \pi^+\pi^-$ events¹⁵ is compared with the prediction using the Malensek parameterization¹⁶ in fig. 15.

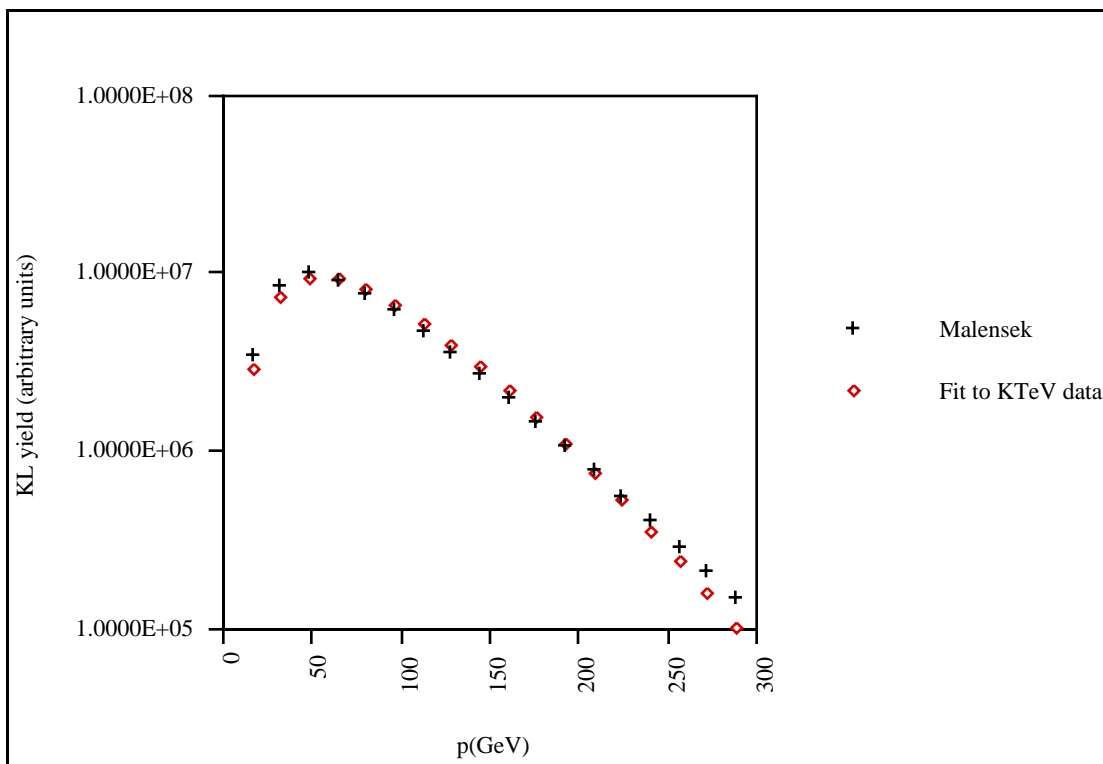


Fig. 15. K_L^0 momentum spectra

4.5 Yields vs targeting angle

The dipole magnets NM2D1 and NM2D2 allow the vertical targeting angle to be changed without changing the position on target. The angle could vary from the nominal 4.8 mrad to 4.0 - 5.4 mrad.

This, in principle, allows some fine-tuning of the relative yields of kaons vs neutrons. Table 9 compares the observed on-line kaon yields with the predicted kaon and neutron yields for the E799 condition. The predicted kaon rates are based on the Malensek parameterization¹⁶. The predicted neutron rates are based on the

data of Engler et al¹⁷. The measured kaon rate is based on the kaon yield from the KTeV on-line reconstruction program. The neutron rate is estimated from the counting rate of the lead-scintillator beam hole veto counter located directly behind the CsI beam holes after subtracting the rate due to kaons.

Table 9. Yields relative to nominal 4.8 mrad targeting angle

Targeting Angle(mrad)	Measured K_L^0 flux	Predicted K_L^0 flux	Estimated Neutron Flux	Predicted Neutron Flux
4.0	1.25	1.22	1.6	1.4
5.4	0.84	0.88	0.7	0.8

4.6 Profile, stability, and position at CsI

The secondary neutral beam stability (target-collimator-CsI system) was monitored by reconstructing $K_L^0 \rightarrow \pi e \nu$ decays using the KTeV detector as shown in fig. 16. The on-line technique during data-taking monitored positions to about 1 mm using the center-of-energy in the CsI calorimeter from $K_L^0 \rightarrow 3\pi^0$ decays. Off-line, after complete detector calibration, we should be able to determine positions at the level of our design goal (200 μ m). These results are still preliminary and the detailed analysis continues.

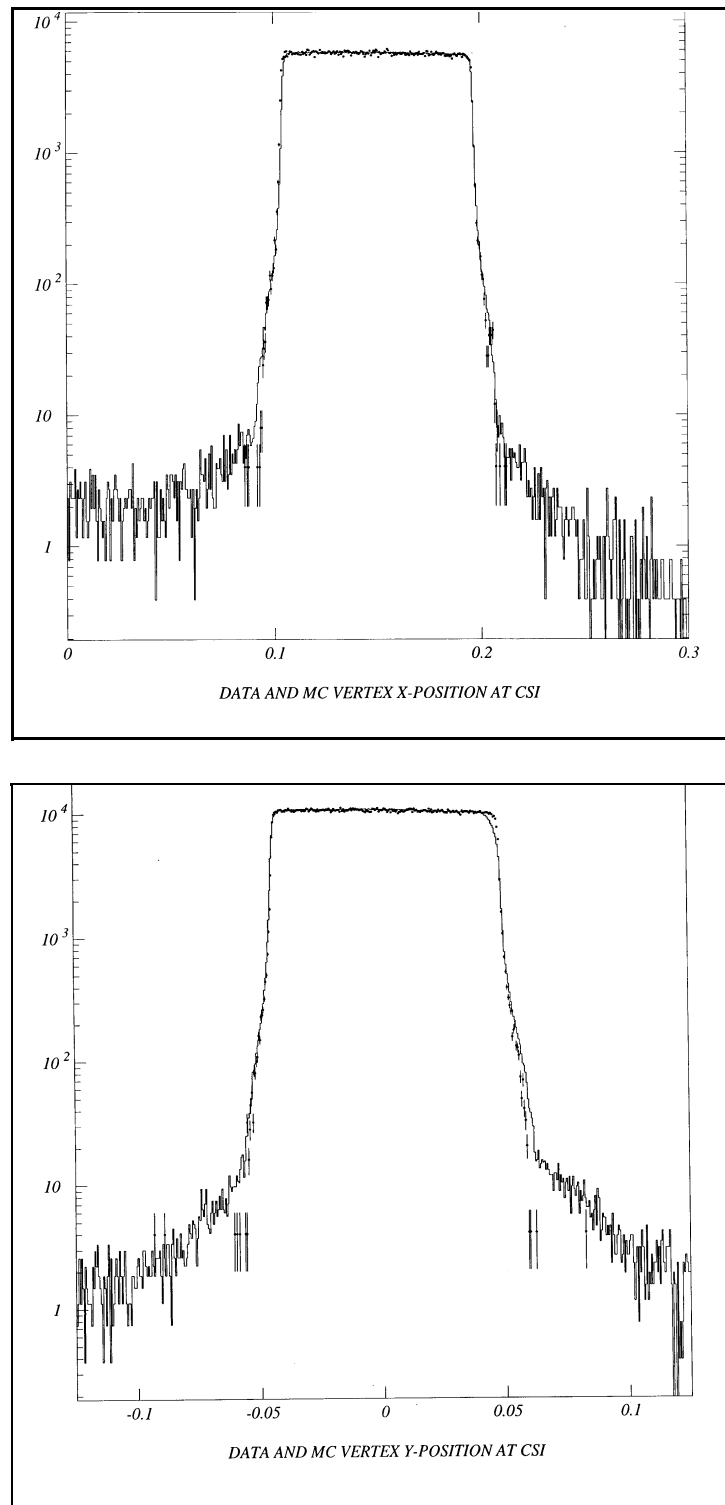


Fig. 16. Horizontal and vertical profiles of the neutral beam at the CsI detector. The histogram is observed data and the dotted graph is the ideal position and shape generated by Monte Carlo simulation.

4.7 *CsI radiation damage*

The KTeV Beam Systems Design Report⁴ contains predictions of the radiation damage to the CsI calorimeter due to two neutral beams passing through the CsI beam holes. Contributions come from the beam itself, neutral K_L^0 decays, and interactions of the beam with material in the detector. These GEANT/FLUKA studies were benchmarked using data from the previous generations of neutral kaon studies in the Meson Center area (E731). The agreement was better than a factor of two. In addition, various detector rates and low-level trigger rates were compared in detail¹⁸. Similar good agreement was found here also. For these experiments radiation damage was a major complication in the physics analysis due to the time variation of the response of Pb-glass crystals near the beam hole. CsI is much more radiation hard than Pb-glass. E731 had radiation damage of the blocks near the beam of 100 rads/week at 0.8×10^{12} protons per Tevatron cycle (minute). The prediction for the KTeV beam was ~ 60 rads/week for E832 at 3.5×10^{12} . The improvement was limited by the use of a regenerator in one of the E832 beams to about a factor of 7. For Meson Center experiment E799-I we observed about 600 rads/week in the worst crystals for 1.35×10^{12} protons per Tevatron cycle. The prediction for E799-II was 250 rads/week at 5×10^{12} or an improvement of about an order of magnitude.

The rates measured during the run were quite consistent with the predictions. For E832 we measured ~ 50 rads/week vs 60 predicted. For E799 we measured ~ 300 rads per week vs 250 rads/week predicted¹⁹.

4.8 *Running with larger solid angles than standard beam*

Since the high-precision beam needs were driven by E832, it was reasonable to question if the specifications might be eased for E799-II, particularly the use of a larger solid angle to obtain more neutral flux for rare decay searches. Initially we tried to increase the standard solid angle (.25 microsteradians) by 1.8x. The concern

was radiation damage to the CsI and its effect on the precision calorimetry needed by E832. This was tried during the first running of E799-II in January 1997. The radiation damage increased by 2.5 over the standard beam in good agreement with the predictions from GEANT/FLUKA. At this time we still had to return to a second long E832 data run and as not all details of the CsI calorimeter response were well understood with regard to radiation damage, the decision was made to retreat back to the standard beam size.

A compromise was to attempt a 1.4x standard beam solid angle for the second half of E799-II later that summer. The 1.4x beam worked well, giving only about 1.6x more damage than the standard beam²⁰.

4.9 Hyperon polarization and final sweeper effects

In the KTeV configuration the primary beam is targeted at 4.8 mrad vertically, so the lambda polarization is horizontal. The first three magnets have vertical fields and rotate the polarization by 270 degrees. So the initial polarization along the x-axis is rotated to align with the z-axis. Then the next magnet (spin rotator) has horizontal fields and rotates the polarization into the \pm y-axis depending on polarity. This polarization information can then be used in the hyperon physics analysis. The polarization of the lambda hyperon was observable in the on-line plots.

A "hot spot" in the CsI activity was found to be due to protons from lambda decay which were steered by the final sweeper about half-way out of the CsI crystals. We attempted to lower the final sweeper current so that the protons were not swept out of the beam hole, however this introduced a large background originating just downstream of the defining collimator which dramatically increased the 4-track trigger rates. Therefore we opted to run the sweeper current high (16kG) and flipped the polarity periodically to minimize the radiation damage from the protons from lambda decays.

5. Alignment

5.1 Alignment concept and design

The design phase played a crucial role in the successful alignment of the beam and experiment. Starting from the complete understanding of KTeV's requirements and ending with details about the alignment and monitoring of each component, a very comprehensive plan was formulated in preparation for the installation of the experiment. The alignment and stability concepts have been incorporated in the KTeV Beam Systems Design Report⁴.

During the design phase, the Fermilab Survey-Alignment-Geodesy Group (SAG) was actively involved with the KTeV collaboration in important areas. A number of issues were addressed:

- determination of the required positioning tolerances between the theoretically desirable and practically achievable;
- early and active participation and support of the SAG group in the design of the components to ensure that the systems could be realistically aligned to required tolerances with a cost-effective effort on the part of the alignment teams; and
- understanding of the positional stability as might be affected by such factors as ground motion and thermal stability.

5.2 Surface geodetic control network

The experiment is constructed in the Fermilab site (accelerator) coordinate system. For historical reasons, this local reference system is referred to as the DUSAF system. For absolute positioning, the horizontal accuracy of the DUSAF system is ± 3 mm. Though adequate for the civil construction and to relate KTeV to the extracted beam system where the primary beam is initially defined, it is not accurate enough for final focusing, targeting, and neutral beam alignment. Therefore, a local KTeV Surface Control Network was developed. In this Surface Control Network, the horizontal and vertical aspects are treated separately. The vertical control network is carried out through the existing Fermilab vertical reference monuments.

The design and optimization of the Surface Horizontal Control Network led to a configuration of polygons with central points and a chain of quadrilaterals to ensure a strong geometric figure. The network consists of a combination of ten survey monuments, placed outside the project construction area, and six vertical sight pipes for transferring coordinates. This network is used to tie NM2 and NM3/4 together. The geometric configuration is shown in fig. 17. The Surface Horizontal Control Network was designed to be observed using both conventional and Global Positioning System (GPS) techniques and tied to the DUSAF system. Pre-analysis and simulations indicated that absolute error ellipses in the ± 0.6 mm range should be obtained. Therefore the Surface Horizontal Control Network is consistent with DUSAF datum, but is locally about five times more accurate than DUSAF. Its accuracy is sufficient not only for strengthening the azimuth constraints and establishing a more precise scale for the underground network through the points transferred from outside, but also for construction and experiment monitoring purposes.

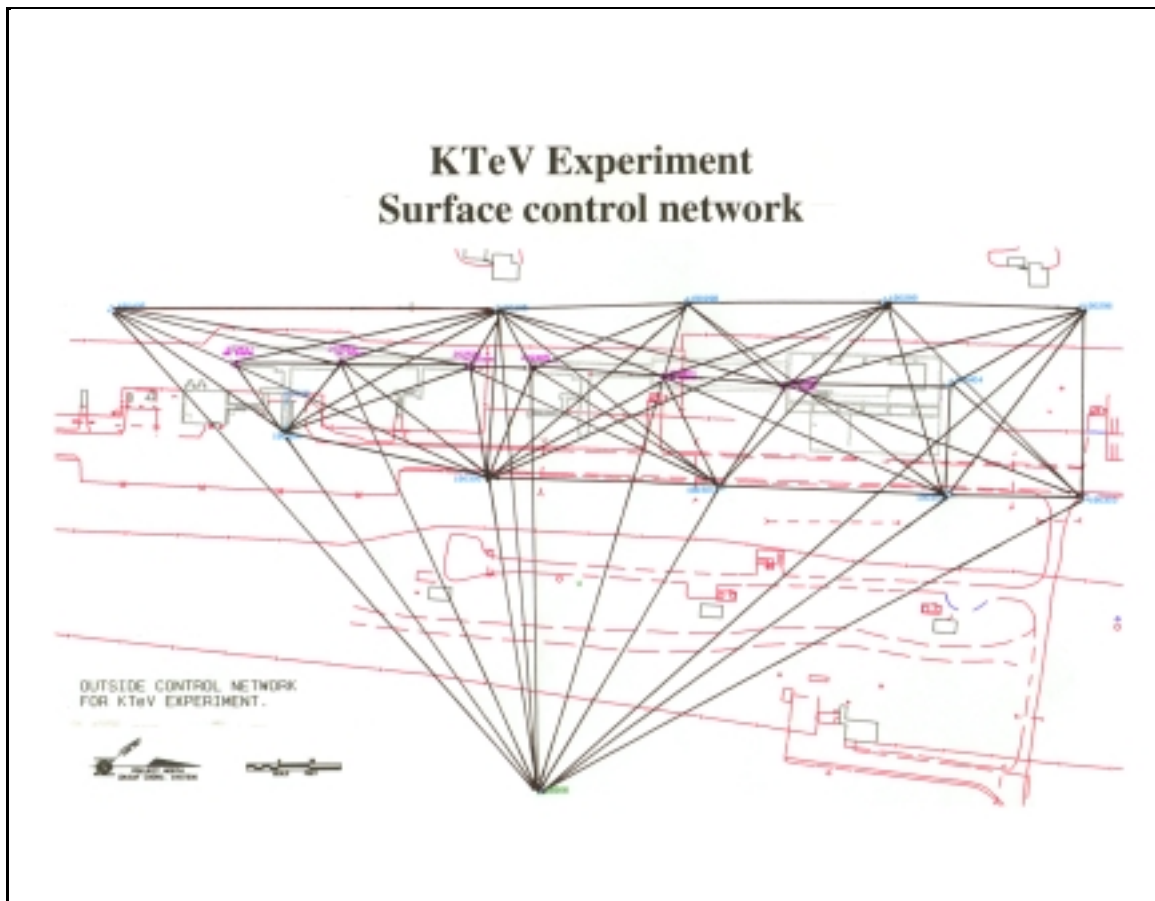


Figure 17. KTeV Surface Horizontal Control Network Phase II

The Surface Horizontal Control Network was implemented in two phases. During initial implementation, it was used by the civil construction contractor to lay out the buildings and by the SAG group for quality control checks of the layout work and monitoring the construction. The second phase, after construction, necessitated another high-precision survey of the network for incorporating the six vertical shafts and transferring surface coordinates to the KTeV Underground Control Network. Figure 18 shows a histogram of the standardized observation residuals. The 95% confidence level absolute error ellipses obtained for all the control points in both surveys were in the ± 0.6 mm range. Coordinates have been transferred from the precise surface network in enclosures with 1/200000 accuracy.

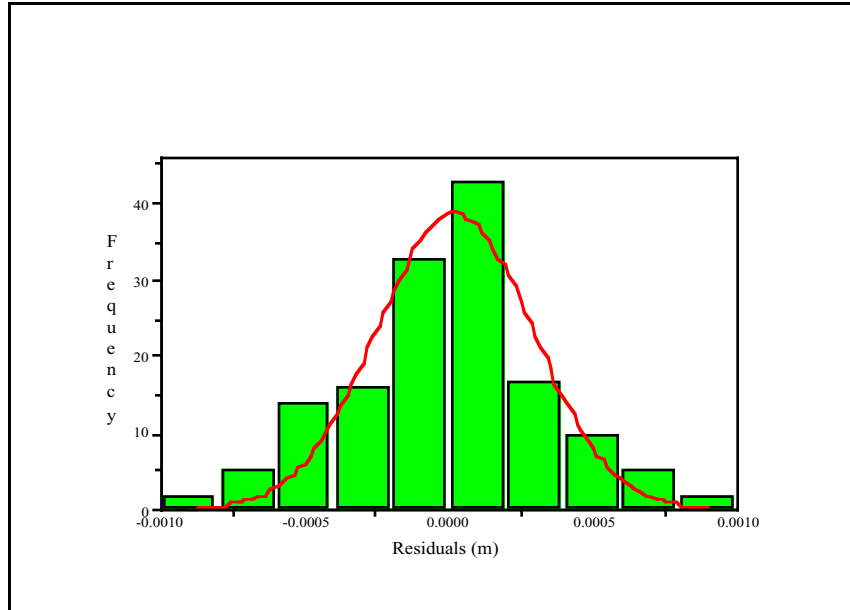


Fig. 18. Surface control network. Histogram of standardized observation residuals.

5.3 High accuracy underground control network

A major requirement for KTeV's alignment is to minimize the relative errors. This calls for a high-accuracy underground control network with very strict and tight tolerances, which makes it possible to establish relative component positions to ± 0.25 mm (2σ) throughout the experiment. It is also the basis for a dynamic monitoring system for relative position checks on components.

The configuration of the network is limited by the shape and the geometry of the enclosures and the experimental hall which dictates that the KTeV underground network be of longitudinal type. The studies carried out led to a framework system based on chains of polygons with central points throughout the NM2 and NM3 enclosures, and the experimental hall. To improve the isotropy of the network and compensate for the weaknesses caused by the poor ratio between some sides of polygons, additional measurements spanning adjacent polygons were added. Redundant observations were needed to ensure quality and uniformity of accuracy. Figure 19 shows the planar configuration of the precise underground network in the experimental hall.

The underground reference control system is defined with respect to monuments permanently imbedded in the enclosure floor, alternating with monuments rigidly attached to walls for improving the overall spatial geometry of the network. This control network consists of 140 monuments, the positions of which must satisfy a number of criteria:

- the points must be easily accessible;
- minimize the number of observations necessary for component positioning and to allow for eventual smoothing routines;
- the density of the points has to be great enough to cover the objects to be surveyed; and
- the network structure must be flexible enough for future needs.

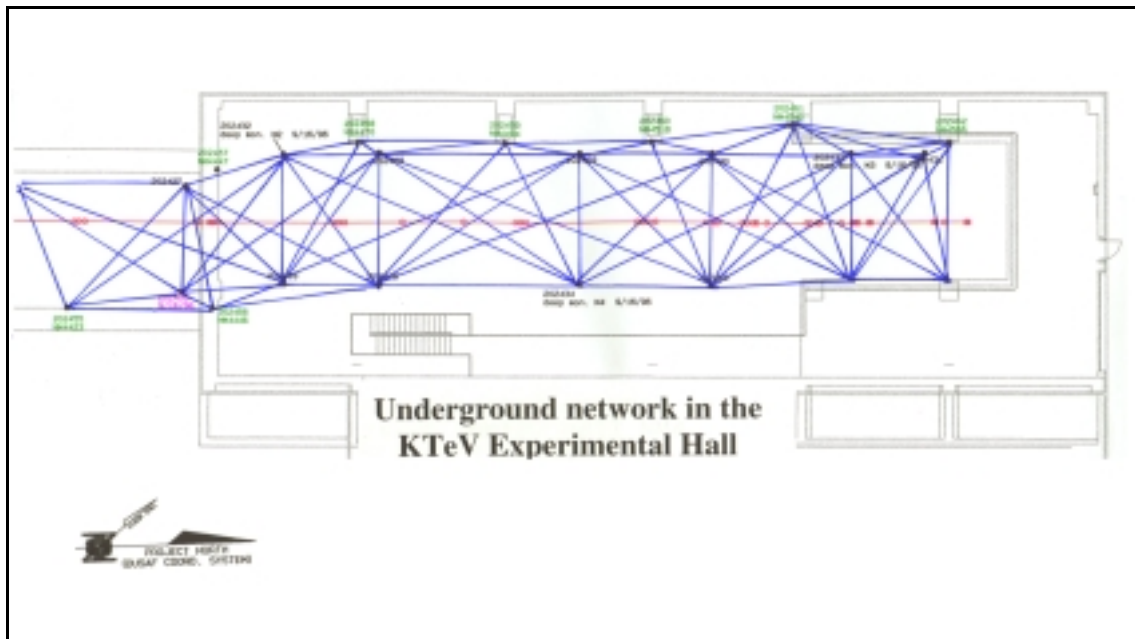


Fig. 19. KTeV Underground Control Network in the experimental hall (NM4)

Network simulations led to the number and location of six vertical sight risers used for transferring coordinates from the Surface Control Network. These points provide azimuth constraints, concurrently controlling the scale of the network.

Tying the control points between the two enclosures by direct observations through the horizontal sight pipe and the beam pipe requires a special procedure involving simultaneous observations with two Laser Tracker instruments and a carefully controlled

environment. The horizontal sight pipe also provides a direct access for checking the relative accuracy between critical components, such as the collimators, in NM2 and NM3/4 at any time.

The underground network is processed as a three-dimensional trilateration network, with distances computed from the Laser Tracker observations. Error propagation analysis indicates that this network should achieve relative accuracies between any control points between the target and the end of the experiment (~200 m) to better than ± 0.3 mm at 95% confidence level. Between 1995-97 the network has been remeasured four times for maintenance and monitoring purposes. Figure 20 shows a histogram of the residuals. We obtained relative errors between control points from the target area and, throughout the network, to the end of the experiment consistently below ± 0.35 mm, at 95% confidence level, as shown in fig. 21.

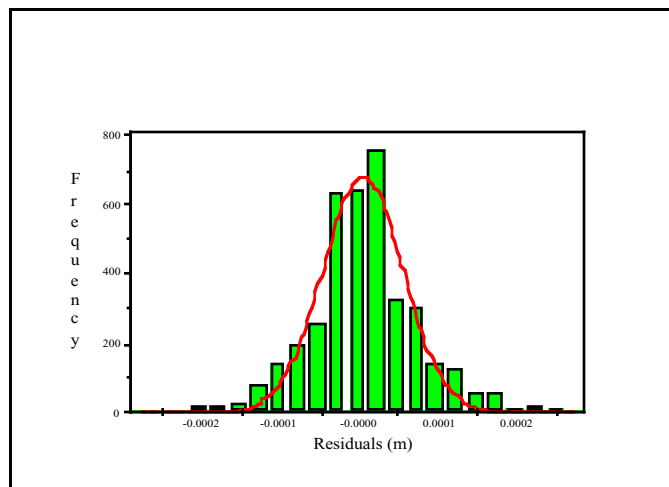


Fig. 20. Underground control network. Histogram of standardized observation residuals.

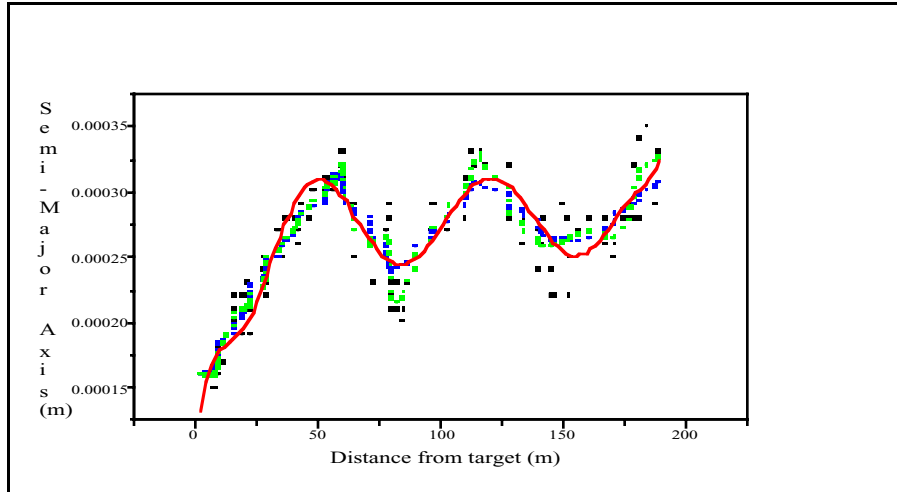


Fig. 21. Underground control network. Semi-major axis of relative ellipses of errors (95%) related to the target.

The vertical reference frame for the underground control is carried out from the surface monuments through the sight risers, and uses precise leveling through the tie rods permanently mounted into the walls of the enclosures and experimental hall. Relative orthometric heights between any two points of the experiment can be determined within ± 0.25 mm at 95% confidence level employing standard procedures and controlling the environment. The vertical reference network has also been re-measured six times, and in each surveying campaign, precision in the range of ± 0.6 - 0.8 mm/km double run has been obtained.

5.4 Monitoring relative positions and stability

After initial determination of the horizontal and vertical control networks, the SAG group implemented a regular schedule for remeasurement of these networks and conducting detailed analysis, including robustness estimators in modeling the data, for detection of displacements or deformations.

In order to provide better stability monitoring for the underground networks, four permanent deep monuments have been built in the NM3 enclosure and experimental hall. Besides providing stable monitoring references closer to the experiment, these monuments also constitute fundamental references for the

underground control by reducing the amount of time it takes to reestablish the network inside the KTeV hall.

5.5 Error budget analysis

Mathematical and statistical analysis has been performed to define the total error budget for the Laser Tracker alignment of the components, and also to determine the contribution of each individual error to the model, based on the differential and variational influence principle. A summary of the major component errors (at 1 σ) is the following:

$$\sigma = \sqrt{\sigma_n^2 + \sigma_m^2 + \sigma_f^2 + \sigma_s^2} = \sqrt{0.143^2 + 0.072^2 + 0.070^2 + 0.050^2} = \pm 0.182 \text{ mm},$$

where:

- σ_n relative errors in the network;
- σ_m control points to fiducials;
- σ_f fiducials to component center; and
- σ_s resolution of the adjustment device.

5.6 Beam stability monitoring systems

The alignment and stability were checked using a variety of methods including remeasurement with the Laser Tracker, on-line and off-line analysis of beam and physics data, and independent hardware designed to monitor relative motion. The tiltmeters and Hydrostatic Leveling System by FOGALE Nanotech (HLS) probes were mounted on a number of critical devices. Monitoring alignment of the neutral beam elements to the required tolerances is critical for the KTeV program. Since the most stringent alignment requirements are relative positions, an on-line dynamic monitoring system is employed. A part of the plan for monitoring the KTeV geometry includes the use of tiltmeters and a HLS. As instrumentation, we employed KERN Swiss NIVEL 20 Tiltmeters that register in two orthogonal directions with a resolution of 0.001 milliradians, and the HLS. Mounted on a number of critical devices, these systems provide information independent of beam data.

The analysis of the data from these stability monitoring systems is also still in progress, and the results presented here are still preliminary.

It was not possible to monitor the target system with the tiltmeters due to excessive radiation. The upstream collimator was monitored, but two tiltmeters failed from radiation exposure. Longer term monitoring of the defining collimator, the spectrometer magnet and the CsI calorimeter was effective. Figure 22 shows the spectrometer magnet rotations and stability monitored over a nine month period. The tiltmeter data indicated that the magnet was stable to an accuracy of about $20 \mu\text{rad}$.

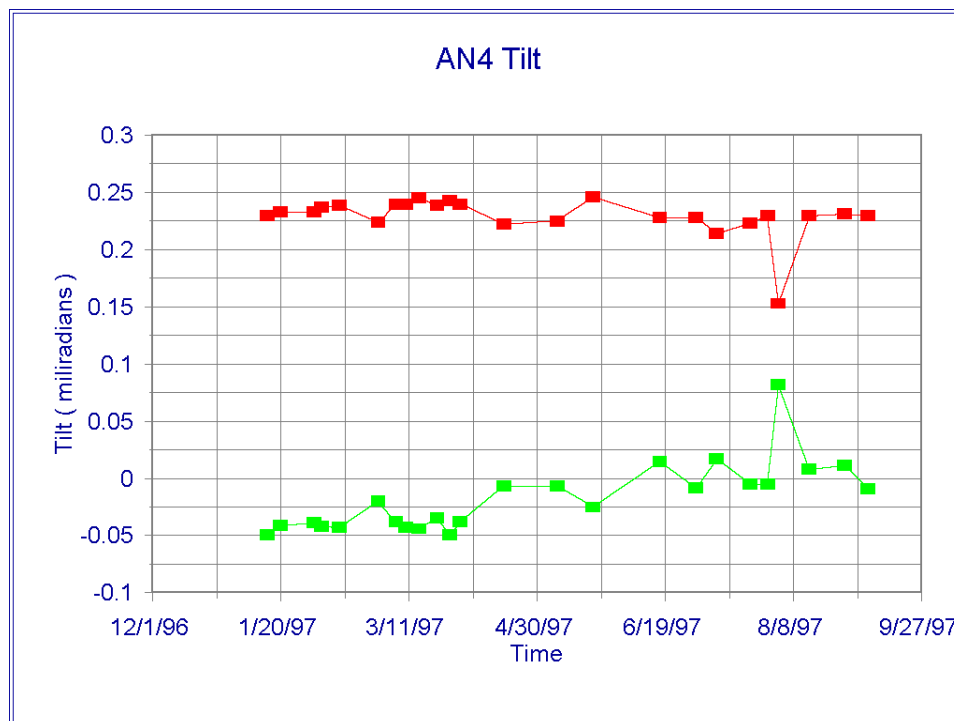


Fig. 22. Lateral and longitudinal rotations of the spectrometer magnet monitored with the Tiltmeter.

The HLS system was initially planned to extend from the target area to the CsI calorimeter. Due to large temperature variations in the target hall compared to the experimental hall (relative variations of order 20°C from magnet power loads), it was not possible to monitor the entire system. Radiation damage problems were also exhibited over the first several months of operation. The system

that was monitored for the last four months of the experiment consisted again of the defining collimator, the spectrometer magnet, and CsI calorimeter. Data from the HLS system was read into the KTeV DAQ system.

In this long-term stability analysis, the spectrometer magnet is used as reference. Figure 23 shows the differential vertical position of the defining collimator and the CsI calorimeter over the four month period. While some small shifts in the angle of the CsI were observed, the relative height of the CsI calorimeter with respect to the spectrometer magnet remained constant to within about 100 μm over this period. The defining collimator was subject to systematic shifts during changeover of experiments, but during periods of running a single experiment (2-3 months) the collimator was also stable to about 100 μm relative to the spectrometer magnet.

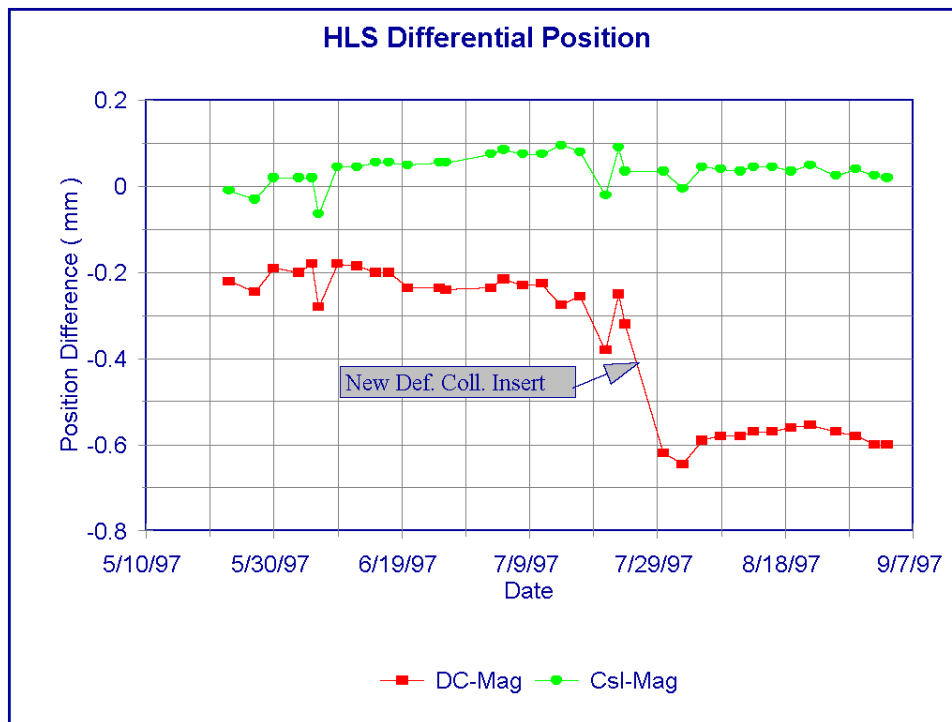


Fig. 23. Vertical position of the CsI detector and defining collimator referred to the spectrometer magnet.

The HLS readout on individual items was subject to apparent shifts of a couple millimeters due to thermostatic fluctuations. Figure 24 shows such a systematic progressive shift exceeding 0.25 mm in

the raw HLS data sample collected continuously over a 250 minute period for analyzing short term stability. However, as shown in fig. 25, differential shifts were very small, in the $10 \mu\text{m}$ range. Note that for the vertical axis of figures 24 and 25, the conversion factor from Volts to linear units is: $0.1 \text{ Volt} = 50 \mu\text{m}$.



Fig. 24 Raw HLS data of the CsI calorimeter, defining collimator, and spectrometer magnet stability monitoring. (Vertical scale: $0.1 \text{ Volt} = 50 \mu\text{m}$)

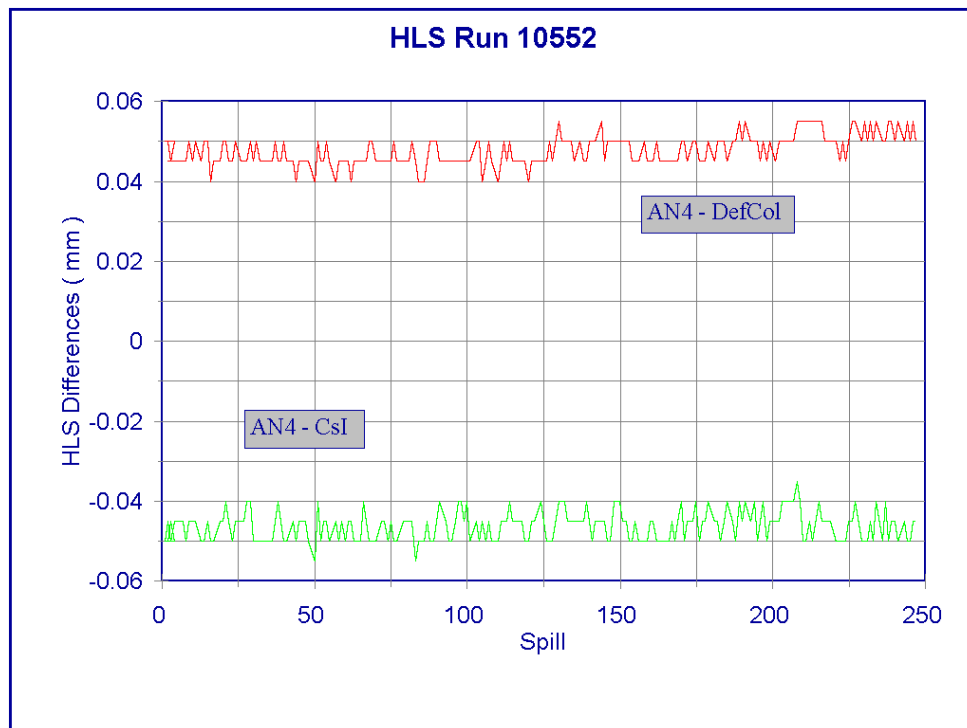


Fig. 25. Stability of the CsI calorimeter and defining collimator referred to the spectrometer magnet over time. (Vertical scale: 0.1Volt = 50 μ m)

5.7 Alignment Conclusions

The network to support the installation and commissioning of the KTeV experiment was, as demonstrated by the initial accuracy of the positions of the primary and the neutral beam with respect to the experiment, an unqualified success. Long-term monitoring based on multiple resurveys and instrumentation monitoring, though still being analyzed, indicates that the geometry of the experiment was very stable. These results represent a major improvement compared to other similar experiments.

6. Past and Future Operations

The beamline was commissioned in the summer of 1996. The experiment began data-taking in the fall of 1996 and ran for approximately one year. Plans are underway for another physics run in the spring of 1999. No major changes are required for the beamline. Some upgrades/repairs are needed in the primary beam instrumentation; the upgraded digital BPM electronics has several shortcomings and needs major re-work and, in addition, the target SEED wire planes are being examined and may have to be repaired. A 20% loss of signal in the beam region was seen. A new insert will be made for the defining collimator to make a single "pencil" beam of about 0.06 microsteradians for the dedicated running to search for $K_L \rightarrow \pi^0 \nu \bar{\nu}$.

Finally, many components of the beam will likely be reconfigured for running with 120 GeV primary beam from the Fermilab Main Injector. The year 2000-2001 is anticipated to be the earliest running with the intense Main Injector beams which will give approximately two orders of magnitude improvement in the sensitivity of the kaon physics program.

ACKNOWLEDGEMENTS

The authors would like to express our gratitude to the US Department of Energy for supporting the construction and maintenance of the beamline over the past fixed target run. We express our deep appreciation to Fermilab for providing all the necessary technical support. We thank the numerous people who helped in all the aspects of this project: the Beams Division, the engineering, mechanical, electrical and alignment groups. We are grateful to many members of the KTeV collaboration who contributed to this performance note with their suggestions and analysis.

REFERENCES

- [1] K. Arisaka et al., KTeV Design Report, Fermilab FN-580, January 22, 1992.
- [2] E731, E773, and E799 Collaborations, Results from the Neutral Kaon Program at Fermilab's Meson Center Beamline (1985-1997), Fermilab-Pub-97/087-E, May 1997.
- [3] L. Gibbons, A Precise Measurement of the CP-Violation Parameters $\text{Re}(\epsilon'/\epsilon)$ and Other Kaon Decay Parameters, PhD thesis, University of Chicago, August 1993.
- [4] V. Bocean et al., KTeV Beam Systems Design Report, Fermilab-TM-2023, September 1997.
- [5] R. Drucker, R. Ford, and G. Tassotto, Secondary Emission Detectors for Fixed Target Experiments at Fermilab, Paper presented at the Third European Workshop on Beam Diagnostics and Instrumentation for Particle Accelerators (DIPAC 97), Frascati, Italy 1997.
- [6] D. Johnson, Fermilab Operations Dept., private communication.
- [7] J. DeVoy, G. Gutierrez, and T. Kobilarcik, Fermilab internal notes on AUTOTUNE program, also see the appendix of Ref 8.
- [8] T. Kobilarcik, Results of Stability Study for the KTeV Beam, Fermilab-TM-2037, January 1998.
- [9] R. Tesarek, KTeV collaboration, private communication.
- [10] Fermilab Radiation Survey Map, Fall 1996.
- [11] R. Ford, private communication.
- [12] L.G. Pondrom, Hyperon Experiments at Fermilab, Physics Reports 122, (1985), 57-172.
- [13] M. Arenton, B. Cox, V. O'Dell, K. Senyo, T. Yamanaka, KTeV internal memo, Details of the $K_L \rightarrow \pi\pi e e$ Analysis, October 1997.
- [14] S. Bright and E. Ramberg, KTeV hyperon group, November 1997.
- [15] P. Shawhan, private communication.
- [16] A. Malensek, Empirical Formula for Thick Target Particle Production, Fermilab-TM-341, October 1981.
- [17] J. Engler et al., Measurement of Inclusive Neutron Spectra at the ISR, Nucl. Phys. **B84** (1975) 70-82.
- [18] T. Alexopoulos et al., Estimation of the E799-II Trigger Rates, KTeV internal note #0235, August 1994.
- [19] A. Roodman, KTeV collaboration, private communication.
- [20] C. Qiao, KTeV internal note #439, June 1997.